Forces controlling the intra-plate stress field: the Alboran Domain and the Eastern Pyrenees during the Miocene

MSc Thesis

Pieter Jeen de Boer

July 2013

Supervisor: Dr. P. Th. Meijer

Universiteit Utrecht

The Mediterranean region evolved due to different stages of extension caused by slab roll-back in a convergent regime imposed by the still continuing Africa-Eurasia convergence. The Betic-Gibraltar-Rif arc defines the rim of the Alboran Sea; the arc and sea together make up an example of such a zone of extension in a convergent regime. The westward migration of the Alboran Domain - caused by a combination of extensional collapse due to increased gravitational potential energy and slab roll-back induced by the retreating slab currently west of Gibraltar - influenced the area in several ways. The extensional collapse is responsible for the thrusting of the Alboran Domain on continental Iberia and the formation of the Betic-Gibraltar-Rif arc. The westward migration itself can be a cause for delaying the onset of the Messinian Salinity Crisis. Here, we focus on the question as to which first-order tectonic forces are influencing the Betic region and we will establish their relative importance. By looking at combinations of these tectonic forces with several finite element model runs, it can be shown that a combination of an Alboran Domain 'high' balanced with Africa-Eurasia convergence results in a zone with a neutral state of stress, vulnerable to westward roll-back related pull. A cessation of this pull can therefore be a direct cause for the closure of the Atlantic corridors due to the overtaking of compressional forces. The eastern Pyrenees are also vulnerable to this same compression. This area is of interest because the model is suitable for investigating the question if a combination of compression due to convergence and tension due to gravitational spreading forces can lead to an additional SW extensional phase. This second phase is presented in the field by Late Miocene extensional basins and volcanism.

Contents

1. Introduction 4
2. Geological background 4
2.1 Geodynamic evolution of the Mediterranean 4
2.2 Alboran Domain 6
2.3 Eastern Pyrenees 7
3. Technical background 9
3.1 Introduction to finite element modeling 9
3.2 Concept of internal boundaries 10
3.3 Gravitational potential energy 11
4. Model setup 12
4.1 Boundary conditions in general 12
4.2 Africa-Eurasia convergence 13
4.3 Western edge slab roll-back 14
4.4 Alboran Domain 15
4.5 Eastern Pyrenees 16
5. Results 17
5.1 Betics 17
5.1.1. Forces individually 17
5.1.2. Combination of convergence and roll-back related pull 18
5.1.3. Combination of gravitational spreading forces and convergence 18
5.1.4. Combination of gravitational spreading forces and roll-back related pull 19
5.1.5. Combining all three involved tectonic forces 19
5.2 Eastern Pyrenees 20
5.2.1. No convergence 20
5.2.2. Adding convergence 20
6. Discussion 31
6.1 Betics 31
6.1.1. Forces individually 31
6.1.2. Combination of convergence and roll-back related pull 32
6.1.3. Combination of gravitational spreading forces and convergence 32
6.1.4. Combination of gravitational spreading forces and roll-back related pull 33
6.1.5. Combining all three involved tectonic forces 34

6.1.6. Model limitations 35
6.2 Eastern Pyrenees 35
7. Conclusion 37
8. Acknowledgement 37
9. References 38
10. Appendices 41
Appendix A: Calculation sum of rotations 41
Appendix B: Choice pole of rotation 42
Appendix C: Extending uncoupled internal boundary 45
Appendix D: Tables of results 47

1. Introduction

The Mediterranean region is a complex area, full of arc-shaped thrust belts and newly formed extensional basins, mainly caused by slab roll-back processes. One of those basins is the Alboran Sea, trapped between the Betic-Gibraltar-Rif arc, which is among the tightest orogenic arcs on Earth. This arc is formed by the Alboran Domain, which was driven westward between the converging African and Iberian plates by some combination of a high gravitational potential energy (GPE) and slab roll-back.

An important time period for this region is the Late Messinian, when the Messinian Salinity Crisis (MSC) occurred (± 6 - 5.3 Ma). This event was involved in the desiccation of the Mediterranean and the closure of the gateways in the western Mediterranean played an important role. A lot of research has been done in this region, with at least one common conclusion: a tectonic force contributed to the initiation of the MSC (Duggen et al., 2003; Hsü et al., 1977; Krijgsman et al., 1999).

In this paper I focus on the question as to which first-order tectonic forces are influencing the Betic region and establish their relative importance. Is it possible to distinguish between slab roll-back and an increased GPE as the main driving force in the area? And how did these forces actually influence the stress field at the time just preceding the Messinian? Could the interplay of these forces be responsible for the closure of the western Mediterranean gateways?

To find an answer to these questions I will use a finite element elastic thin shell model which incorporates tectonic forces in various ratios to create different solutions for the palaeo-stressfield. Additionally I will look at a solution for the anomalously high elevation of the Eastern Pyrenees in a similar fashion. This is included in the same study, because insight in this region can be achieved with a similar model, based on a combination of gravitational spreading forces and plate-tectonic forces.

2. Geological background

To get a better insight in the regions of interest, the Alboran and the eastern Pyrenees, I present a short summary of the geodynamic evolution of the Mediterranean, marking the main events of interest for this thesis. I will follow the evolution described by Jolivet et al. (2006) because I take the plate boundaries of their late Messinian reconstruction (Fig. 1) as the basis for my model. Especially the time just preceding and during the Messinian is of interest, because of the search for a tectonic cause responsible for the onset of the MSC. Furthermore, I will describe the Alboran Domain (Fig. 2) and the eastern Pyrenees (Fig. 3) in more detail to get acquainted with some structural aspects of those regions.

2.1 Geodynamic evolution of the Mediterranean

The isolation of the Mediterranean region started in the Late Eocene – Early Oligocene (35-30 Ma) by progressive locking of oceanic lithosphere between two collision zones. The first collision occurred between Africa-Arabia and Eurasia in the east, and the second one between Iberia and the African plate in the west. This is all caused by the SSW-NNE directed convergence between Nubia and Eurasia at that time (Rosenbaum et al., 2002). Jolivet & Faccenna (2000) suggest that due to this collision the convergence started to slow down, creating the opportunity for slab retreat processes to become predominant.

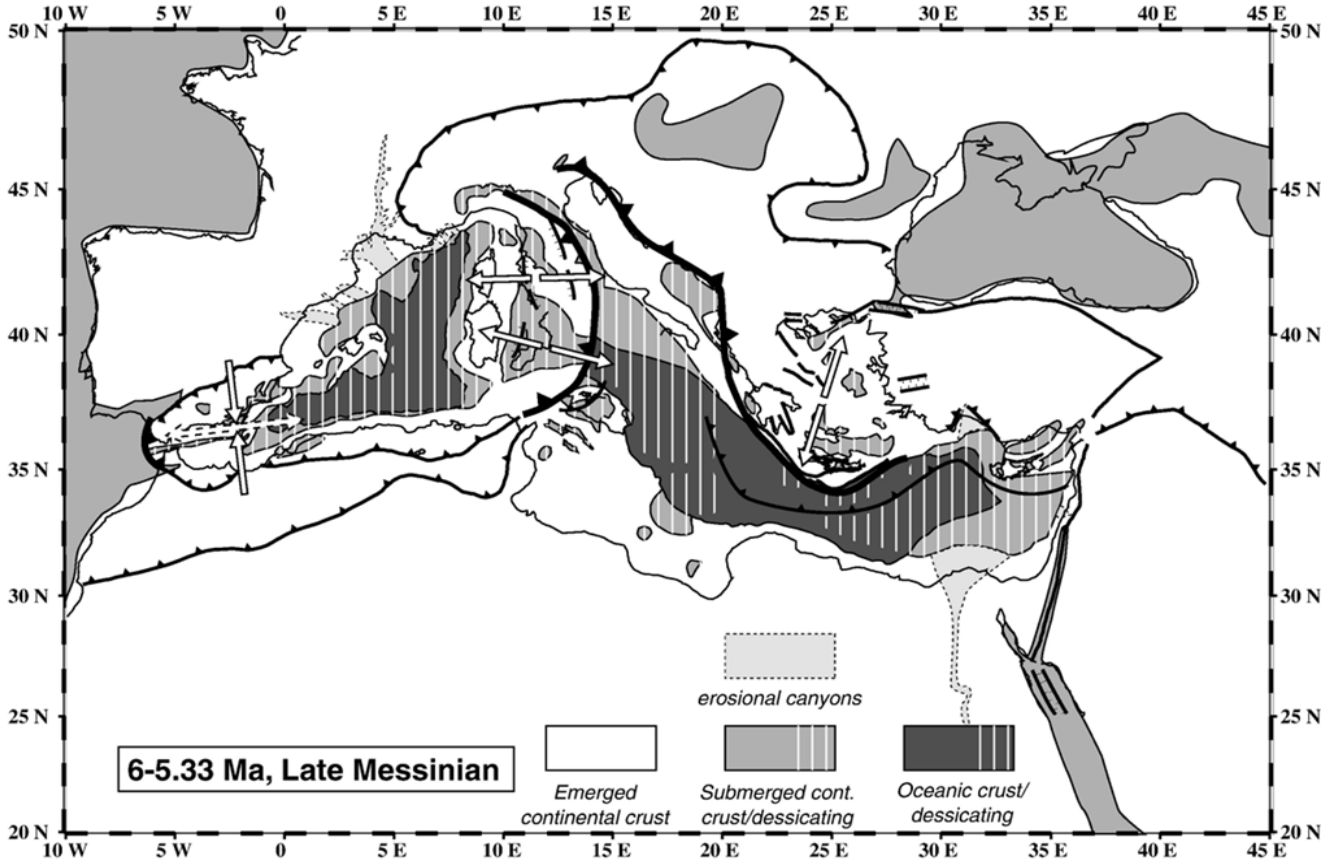

Figure 1: Reconstruction of the Mediterranean region during the Late Messinian proposed by Jolivet et al. (2006). I digitized the Betic-Rif thrust front and used this as an internal boundary in my mesh.

In several regions the regime changed from compressional to extensional, starting with the opening of the Liguro-Provençal Basin (28Ma) and the formation of oceanic crust during the Aquitanian (23 Ma) as well as the formation of extensional structures in the Alboran and Aegean Sea. Slab retreat continued in an outward motion until the Langian (15 Ma), when the subduction zone started to tear and rupture into several pieces (Spakman & Wortel, 2004). The most important piece for this paper is the east-ward directed Betic-Alboran slab retreating to the west below the Betics (Lonergan & White, 1997). During the Serravallian (14 Ma), the connection with the Indian Ocean is lost and oceanic influx can only be achieved at the Betic and Rifian gateways. From the late Tortonian, an uplift of the basin basement is recorded in the Alboran region (Vissers et al., 1995) and at 8 Ma, just preceding the Messinian (7.2-5.3 Ma) the slab retreat process ceased in the Betics (Jolivet et al., 2006), based on the disappearance of back-arc extension in the Alboran Domain which has mostly stopped at that time (Krijgsman & Garces, 2004).

At this stage the N-S compression due to the Nubia-Eurasia convergence could take over as the predominant process. In the central Mediterranean, extension continued in an east-west direction resulting in the opening of the Tyrrhenian Sea. At the same time the gateways to the Atlantic nearly closed, resulting in the onset of the MSC, which culminated in the desiccation of the Mediterranean. Some connection must have remained open to explain the amount of deposited evaporites during the Messinian. Re-opening of the connection through the Gibraltar gate led to the refill of the Mediterranean (Hsü et al., 1977) known as the Zanclean Flood. No further major tectonic changes are

observed from the Pliocene onwards, except the continued opening of the Tyrrhenian Sea and later the formation of the Calabrian arc.

2.2 Alboran Domain

The hinterland region comprising the Alboran Sea and the Internal Betics and Internal Rif, constrained by the thrust zones surrounding it, is called the Alboran Domain (Fig. 2). The eastern border of this area is not well constrained. The Alboran Domain is made up of rocks from different paleogeographic realms than those of the external thrust belt, and it is not fully known how and where the Alboran Domain originated. Platt et al. (2013) describe that it is thought that the Alboran Domain has separated from Africa and Iberia towards the end of the Early Jurassic, due to rifting which initiated in the Triassic.

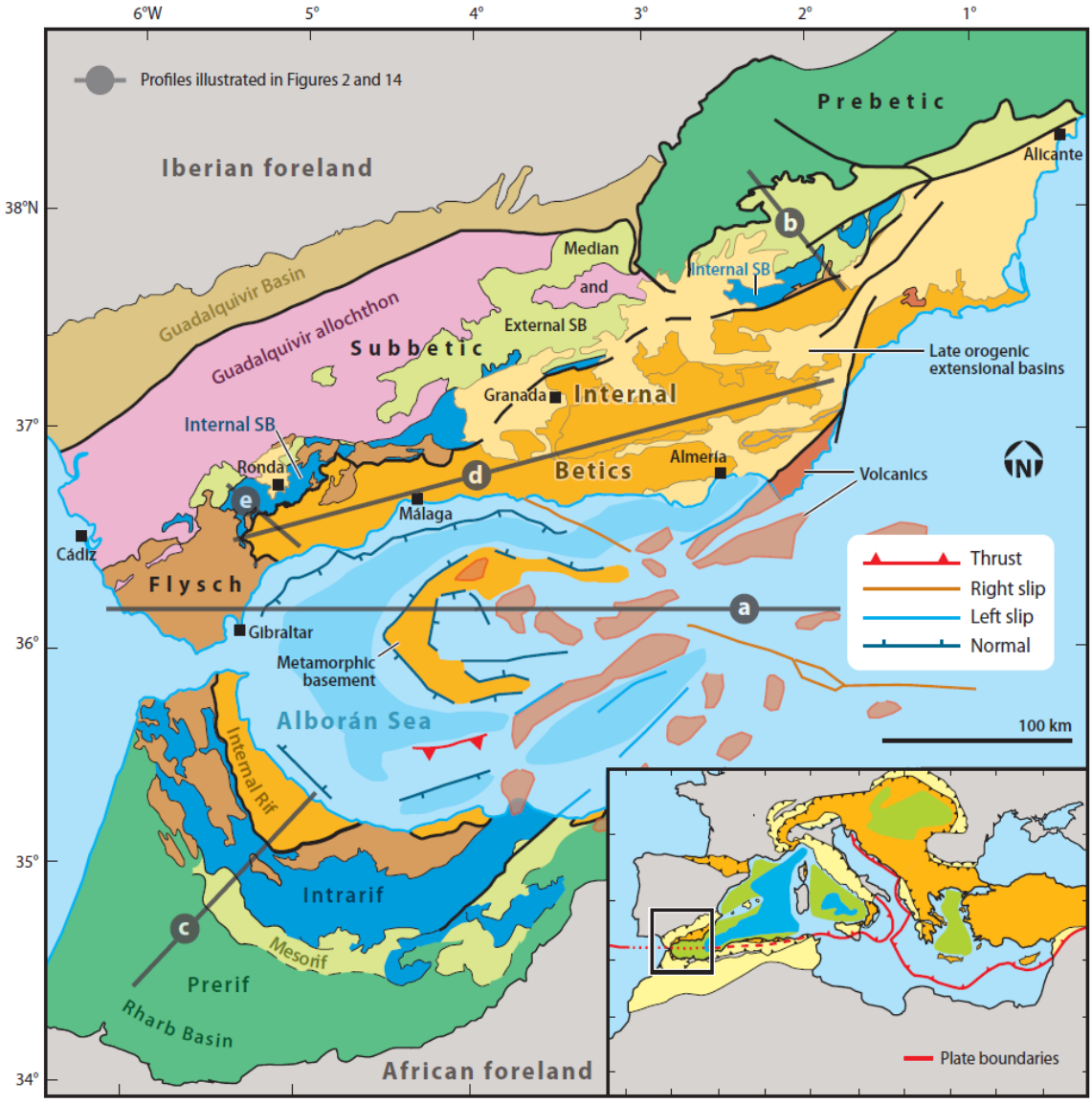

Figure 2: Tectonic map of the Betic-Gibraltar-Rif arc and Alboran Sea (Platt et al., 2013).

The Domain has migrated 200 to 300 km westward since the Oligocene (Martínez-Martínez & Azañón, 1997) this motion came to an end around the Middle Miocene (Sissingh et al., 2008). The boundary between the Internal and External zone could accommodate this westward motion and was mainly active during Burdigalian time (Platt et al., 2013). Extensional collapse and subsidence of the Alboran Domain occurred mainly during the Early Miocene (Platt et al., 1998; Sissingh et al., 2008; Vissers, 2012) and continued at a reduced rate through the Middle and Late Miocene (Watts et al., 1993). The increased gravitational potential energy (GPE) of the Alboran Domain originated during subduction of the African plate below Eurasia in the Oligocene. One of the theories is that the mantle part of the Domain was subducted along with the African plate, while the crust remained at the surface. When slab roll-back initiated, this uplifted piece of the Domain migrated westward and collapsed over time (Bezada et al., 2013). Another possibility is that the westward driving mechanism is the GPE of the Domain itself (Platt et al., 2003). The calculated GPE contrast per horizontal meter of contact between the Alboran Domain and the continental lithosphere of the African and Iberian continental margins is ~5.1 x 10^{12} Nm^{-1}, which is equivalent to ~2.5 times the driving force generated by a mid-ocean ridge (Platt, 2007). Platt et al. (2013) suggest that this driving force is sufficient to drive extension in the Alboran Domain and thrusting of the Domain onto the surrounding continental margin.

Inserting the Alboran block between southern Spain and Morocco closed the Oligocene Tethys marine corridor but caused the opening of new gateways (the Miocene Betic and Rif corridors) by formation of a foredeep surrounding the Betic-Gibraltar-Rif mountain chain connecting the Mediterranean and the Atlantic Ocean (Duggen et al., 2004), see figure 10 for an impression.

2.3 Eastern Pyrenees

The formation of the Pyrenees was not described in section 2.1, because there orogeny occurred well before Oligocene times. The Iberian Peninsula was a separate microplate between Africa and Europe. The convergence of Africa with Europe resulted in the continental collision of Iberia with Europe and the formation of the Pyrenees during the Paleogene (Vergés et al., 2002). At around 42 Ma (Eocene), contraction in the Pyrenees ceased, and Iberia became reattached to Eurasia (Platt et al., 2013).

The opening of the Western Mediterranean (~28Ma) corresponds to a first post-orogenic phase of extension in NW-SE direction. Many normal faults with a strike perpendicular to this direction can be found in the Gulf of Lion adjacent to the Eastern Pyrenees (Mauffret et al., 2001). The Roussillon and Conflent basins are onshore manifestations of this extension, see figure 3 (Gunnell et al., 2008). The Emporda and La Selva basin, including the fault system surrounding them, is of Late Miocene to recent age (Lewis et al., 2000). The normal faults bounding these basins have a strike perpendicular to the normal faults corresponding to the first post-orogenic phase of extension. The age and the different orientation indicate the occurrence of a second stage of extension in NE-SW direction with a different tectonic origin. Late Neogene to Quaternary volcanism in the region, first occurring ~10Ma ago in the Emporda basin supports this second stage of extension.

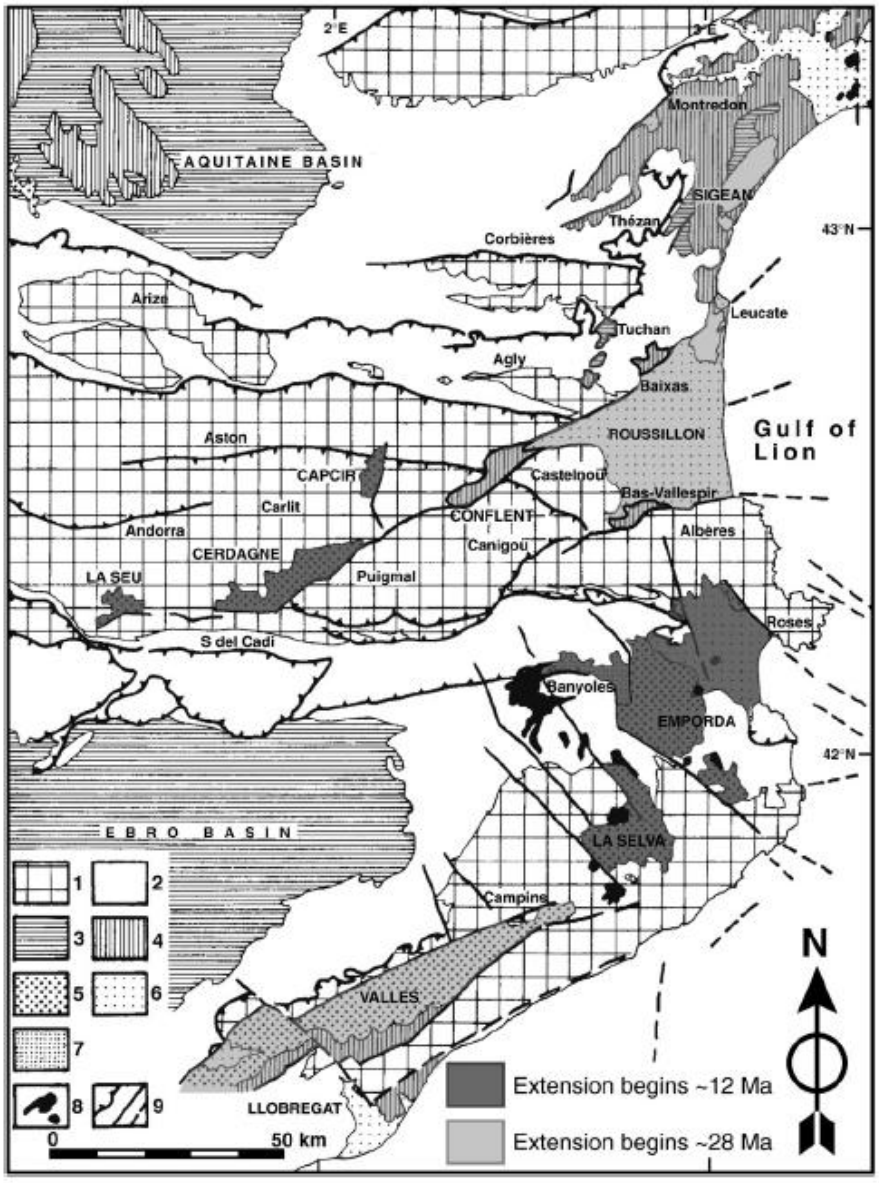

Figure 3: Structural map of the eastern Pyrenees (Gunnell et al., 2008)*. Most important feature is the age and orientation of the extensional basins and the faults surrounding them. The orientation of these faults is key to the stress patterns in my model.*

The origin of this second stage of extension is not known, but Gunnell et al. (2008) relate this to a missing lithospheric root beneath the Eastern Pyrenees. This missing lithosphere is clearly visible east of 2.5°E in their 2-D profiles, two of these profiles are shown in figure 4. These profiles are constructed with an optimization procedure (Zeyen & Fernàndez, 1994) based on a regional set of raw data for surface topography, free-air gravity, geoid and heat flow.

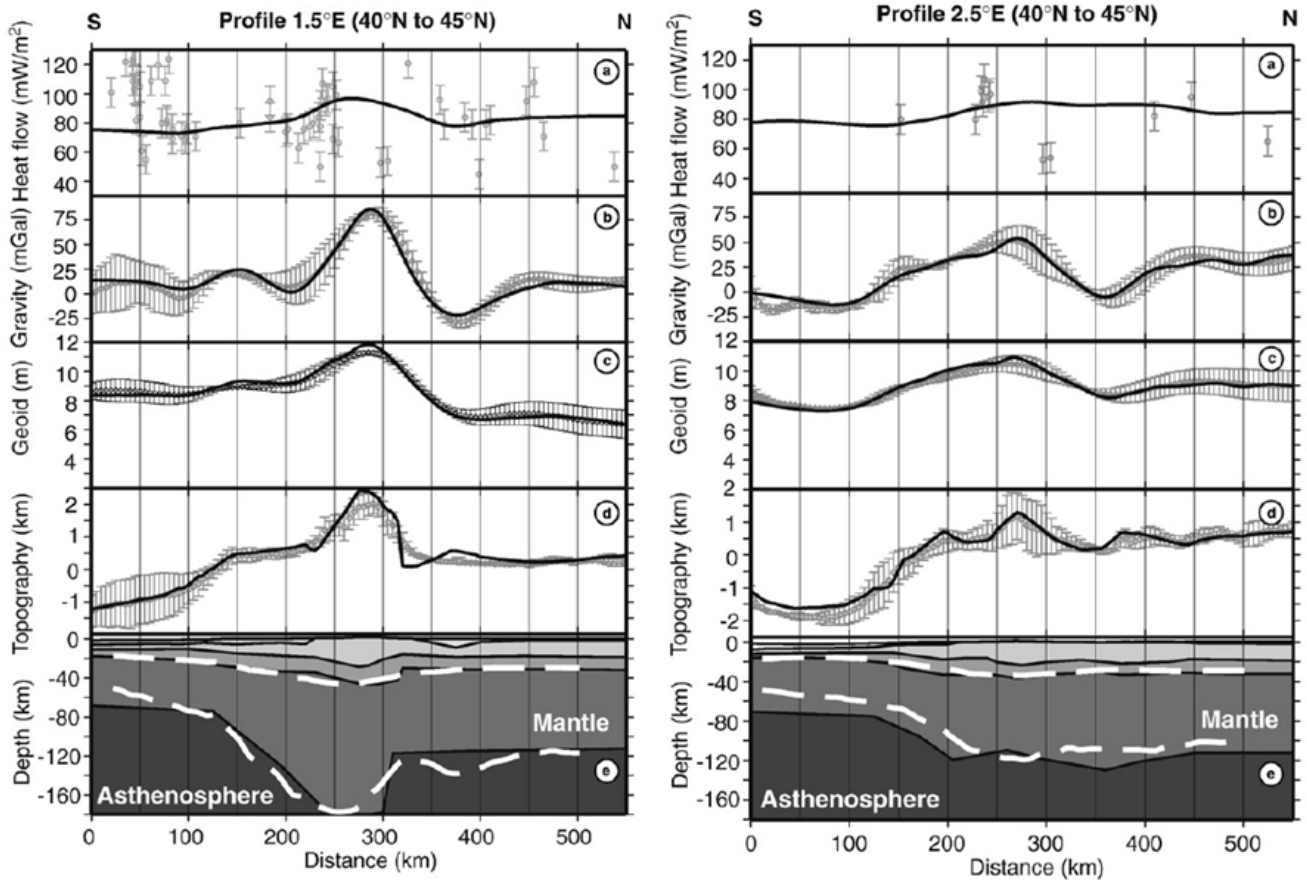

Figure 4: 2-D models of lithospheric structure in the eastern Pyrenees (Gunnell et al., 2008)*. A missing lithosphere is clearly visible at 2.5°E.*

3. Technical background

In this section I will describe some aspects of the finite element model which are of crucial importance for this work. I will not describe any geological details in this part, but as it can still be counted as background information, I will call this the technical background, starting with a short introduction about finite element modeling.

3.1 Introduction to finite element modeling

The finite element calculations are performed with the program GTecton which is developed by R. Govers. The finite element method is a numerical technique for finding approximate solutions to complex problems which cannot be solved by hand. A finite element model is a discrete representation of a continuous part or problem which needs to be analyzed. The object of interest can be subdivided into elements, and each element is made up from several nodes. Figure 5 shows an element with three nodal points to explain the principle of finite element modeling (bottom figure). When loading (p) is applied, the response in every node is calculated and passed on to the next element at its interconnecting node (Fig. 5, top figure). Each nodal point has up to six degrees of freedom (DOF), three components of translation and three components of rotation. The number of

degrees of freedom can be less, depending on which type of element you use. Elements are combined in a finite element mesh. In order to transfer the forces through the mesh, all elements should be interconnected. An exception to this is explained in the next section.

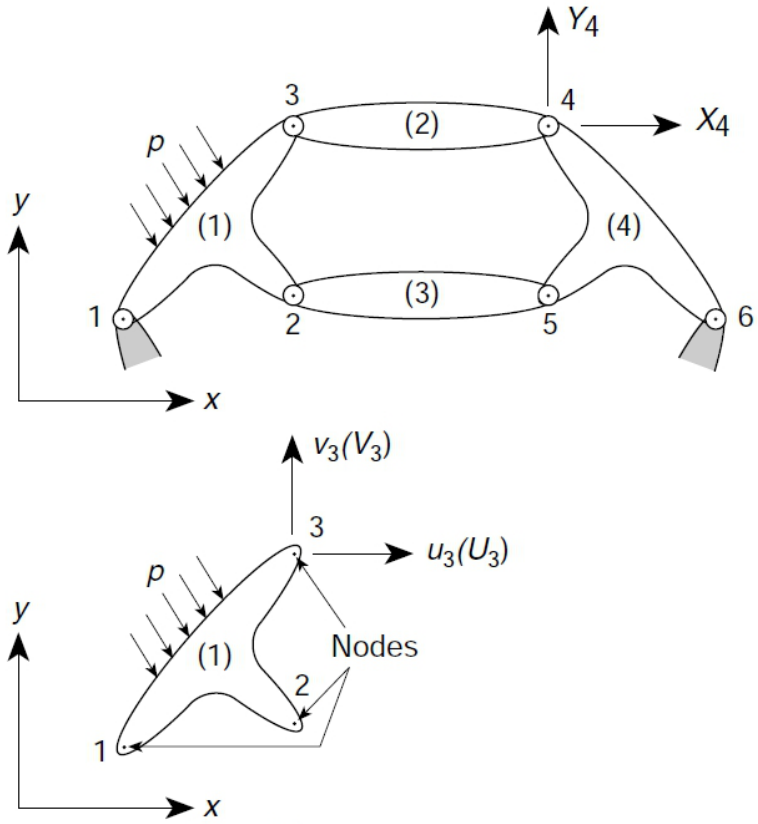

Figure 5: A schematic element used to explain the basic principles of finite element modeling (Zienkiewicz & Taylor, 1977).

3.2 Concept of internal boundaries

By inserting an internal boundary into the mesh the opportunity is created to apply a load to a boundary inside the mesh, instead of only at the outside boundaries. The internal boundary in the resulting mesh is based on a paleogeographic reconstruction of the Late Messinian (Jolivet et al., 2006). The correct representation of the shape of such a boundary results in a finer mesh, necessary to transfer the forces in a correct manner. This is the reason why the internal boundary, at least a large part of it, is clearly visible in the resulting mesh (Fig. 6).

Another important function of the internal boundary is that a node on such a boundary can be split into two nodes, while both nodal points have the exact same geographical position. When you uncouple a series of points in this way, forces cannot pass through this portion of the boundary. We call this an uncoupled boundary. When a load on this boundary is applied, one needs to choose on which side this load will have an effect. If you relate this to a retreating subduction zone, a load can be applied on the overriding plate, leaving the down going plate free, transferring no force from one to the other. Imagine this like an arc-shaped tear in the middle of a piece of paper, you can pull the inside of the arc-shaped tear over the rest of the paper.

Within GTecton it is also possible to work in a reversed order. Once you have uncoupled the entire internal boundary, you can couple each segment of the boundary again in the final stage of the model, looking at the interaction between for instance convergence and changing types of internal boundary conditions for each segment.

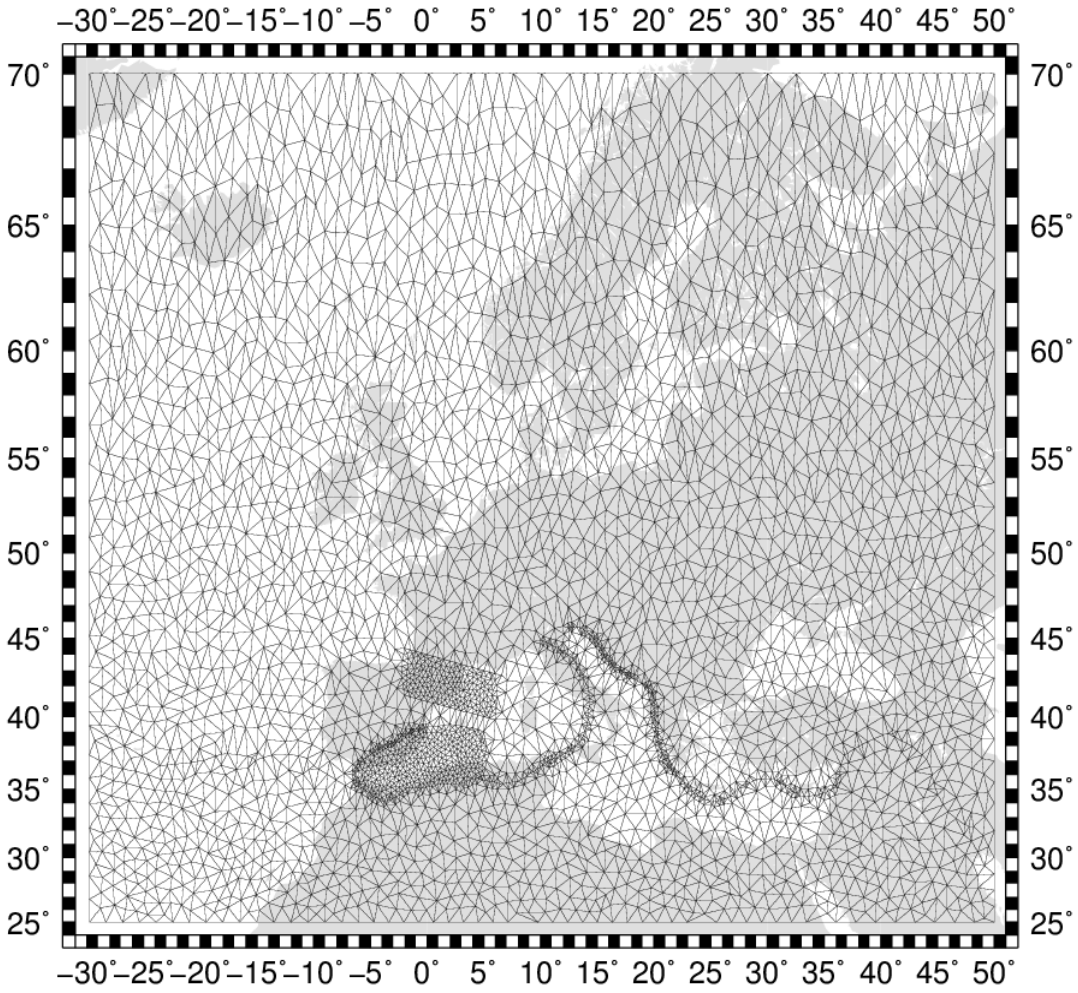

Figure 6: display of entire mesh to show the outer limits. The snake-like figure in the Mediterranean represents the internal boundary digitized after Jolivet et al. (2006)*. The internal boundary of* Bird (2003) *is located between the Atlantic and the Gibraltar Strait and again near Turkey, is less visible. There are two parts where I introduced a finer mesh, the first covering the Alboran Domain and the second covering the Pyrenees.*

3.3 Gravitational potential energy

Gravitational spreading forces such as those thought to play a role in the Alboran Domain are controlled by the density structure of the entire lithospheric column. To simulate these spreading forces in the model, I will use a topographic high, which should not be taken as the absolute level of uplift, because it also comprises the buoyant forces in the lithosphere. We can simply consider such a topographic high compensated by a root to the crust given that (1) we calculate depth-averaged intra-

plate stress (2) the lithospheric structure of the Alboran in the Messinian is uncertain and (3) we are interested in establishing first-order effects of a high in gravitational potential energy. The integration of the effect of topography in the finite element calculations is done by taking into account horizontal body forces that are proportional to gradients in the moment of the density anomalies (Meijer, 1995).

When you compare a local high with its relative lower surroundings, the difference in pressure distribution results in outward spreading. Figure 7a shows a situation in balance, which is made up of contributions due to isostatic compensation at the base of the crust. Constant, temperature independent, densities for crust and lithospheric mantle are used. Calculated are horizontal intra-plate stresses, deviating from lithostatic state and averaged over a chosen reference thickness (Fig. 7b).

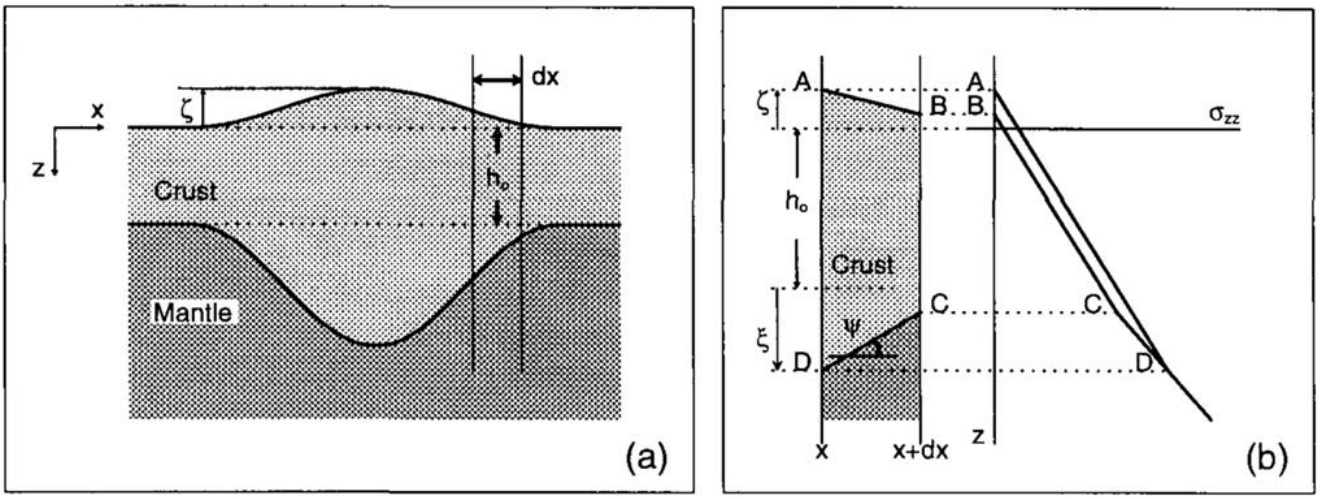

Figure 7: (a) Schematic cross section perpendicular to the strike of a mountain range (b) segment of the cross section showing the variation of the vertical principal stress with depth. This variation of principal stress caused normal faulting to occur in the mountain (Meijer, 1995).

4. Model setup

Before I will describe the choices I made for each force individually, let us have a look at the model in general.

4.1 Boundary conditions in general

The mesh created with Triangle is a large rectangle; from latitude -29.77° to +50° and longitude 25° to 70° (see Fig. 6). The extreme large extent, far beyond the Iberian Peninsula, was chosen to be able to look at more aspects of the entire Mediterranean region in the future, as well as to prevent boundary effects from interfering with the stress-pattern of the Mediterranean.

To get a valid result, some constraints need to be imposed on the mesh boundaries, to allow for a unique solution. The top-left and top-right corners of the mesh have a fixed position, while the northern boundary of the mesh in between those points can move freely in a longitudal way (east to west). The eastern and western boundary of the mesh can move freely in a latitudinal way (north to south), including the points located on these borders originating from the internal boundaries. All

other points in the mesh, including the southern border, are free to move in any direction, as long as they are not restricted by the coupling or uncoupling of the internal boundary.

The internal boundary which represents the African-European plate boundary is a combination of the digitized points of Bird (2003) and the thrust front present in the paleographic reconstruction of Jolivet et al. (2006), which I digitized with the program Gplates (Boyden et al., 2011). Bird's boundaries are used from the Atlantic oceanic spreading ridge until the triple junction west of Gibraltar and again from east of Cyprus until the eastern boundary of the mesh, half-way the Arabian Peninsula. The combination of present-day plate boundaries and reconstructed ones from the Messinian, can be validated by the fact that the actual first-order displacement of the boundary has not been large. Another remark is that I simplified Birds boundaries around the Azores near the Atlantic oceanic spreading ridge for computational reasons, but due to its position far to the west this will not influence the Betic or Pyrenean region.

An extra contour is built in on the eastern side of the Betics and one enclosing the Pyrenees. Due to the presence of these contours the mesh grid size in these regions can be adapted. The location and size of these contours is arbitrarily chosen, and the boundaries themselves are coupled and will therefore not influence the results.

The Mediterranean lithosphere is represented by an elastic thin shell; with a uniform thickness of 100km. Values of $7*10^{10}$ Nm^{-1} for the shear modulus and 0.25 for Poisson's ratio are used, as well as a reference crustal thickness of 35 km. Furthermore the following temperature-independent densities are used for crust: 2800 kg/m^3; and for mantle: 3200 kg/m^3.

4.2 Africa-Eurasia convergence

The convergence between Africa and Eurasia is taken to correspond to a force in the order of 10^{12} Nm^{-1}, acting as a ridge push on the southern border of the mesh. Natural point of application would be a rigid northern Africa, but previous work has shown that the exact point of application is not relevant (P. Th. Meijer, personal communication). The exact value of the force is not relevant as well, changes in magnitude are only inferred to get a stronger or weaker response of the stress field to the convergence, and these values are not based on any theoretical ground.

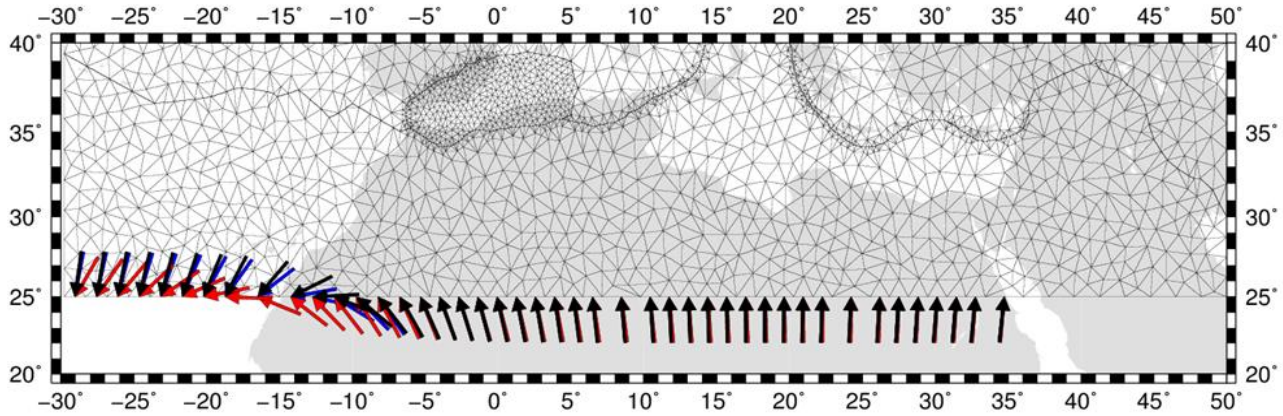

Figure 8: the three different orientations of convergence. The rotation pole used in this model (black arrows) is a subtraction of the one found by Vissers & Meijer (2012) *(blue arrows) and* Calais et al. (2003) *(red arrows).*

The rotation pole for the Africa-Eurasia convergence used in the models is: 21.92° N; 12.56° W; rate 0.102°/Ma . This rotation pole is a combination of the 19.589 Myr average pole of Vissers & Meijer (2012) and subtracting the pole for the last 3.16 Myr of Calais et al. (2003), by the method explained in Appendix A. As shown in figure 8 the orientation of convergence is nearly the same in the African continent. The major difference is the change in position of convergence turning direction from north to south, but this flip has no large effect on the geometry of the stress pattern in and around the Betics, as can be seen in Appendix B.

4.3 Western edge slab roll-back

The exact geographical position over time of the eastward subducting slab is difficult to define. But from the age and composition of volcanic rocks a marked shift in the geochemistry of mantle-derived volcanic rocks can be seen, reflecting a change from subduction-related to intraplate-type volcanism. A plausible mechanism for this shift is the westward roll back of subducted lithosphere (Duggen et al., 2003). The exact shape and position of the slab proves not relevant for the first-order characteristics of the stress field. An outward westward pull at an internal boundary can translate trench retreat to a force in the overriding plate. This principle is also explained in section 3.2.

Tomographic imaging shows that there has been a connection of the slab to the surface below the Betics in the past (Spakman & Wortel, 2004), but at present there is a gap up to 75 km depth (Bezada et al., 2013). See figure 9 for a cartoon based on tomography displaying the 3D geometry of the slab. Since it is not precisely clear when this piece of the slab lost its connection, it will not be implemented as a pull on the overriding margin in the model. I have looked into a model which implemented this extra pull, but it plays no significant role, as can be seen in Appendix C.

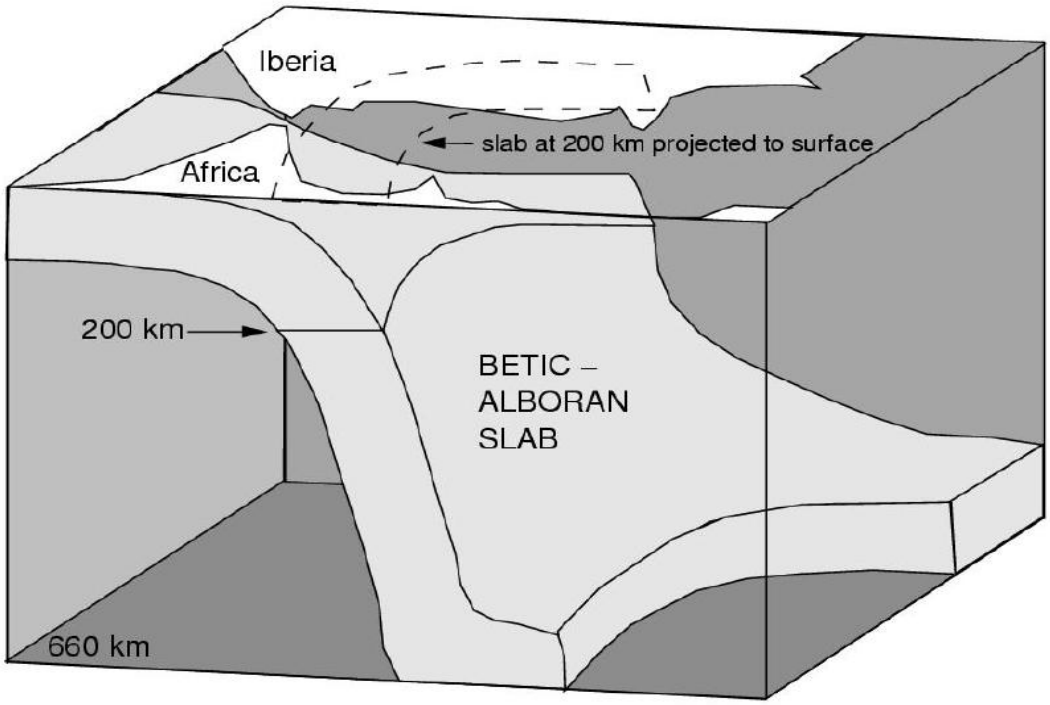

Figure 9: Cartoon displaying an interpretation of the 3D geometry of the area below Alboran Domain, after Spakman & Wortel (2004).

4.4 Alboran Domain

The exact geographical position of the Domain over time is hard to establish. A paleogeographic reconstruction for the Langhian-Serravallian by Sissingh et al. (2008) gives a good example how the area could have developed (Fig. 10), which is already close to present position. An important thing to note is that in this reconstruction only the solid ground of the Alboran Domain is visible as the area which collapses and extends over time, while in my model the region of elevated gravitational potential energy also covers the directly adjacent marine parts, here shown to be dominated by thrusts.

The shape of the Domain used in the models originated by applying the thrust zone as an outer contour, and rounding of this shape at the eastern border to get a kind of elliptical body with a ENE-WSW orientation. The crest points were chosen in the middle of this body in the same orientation, visible in the model results as a straight line.

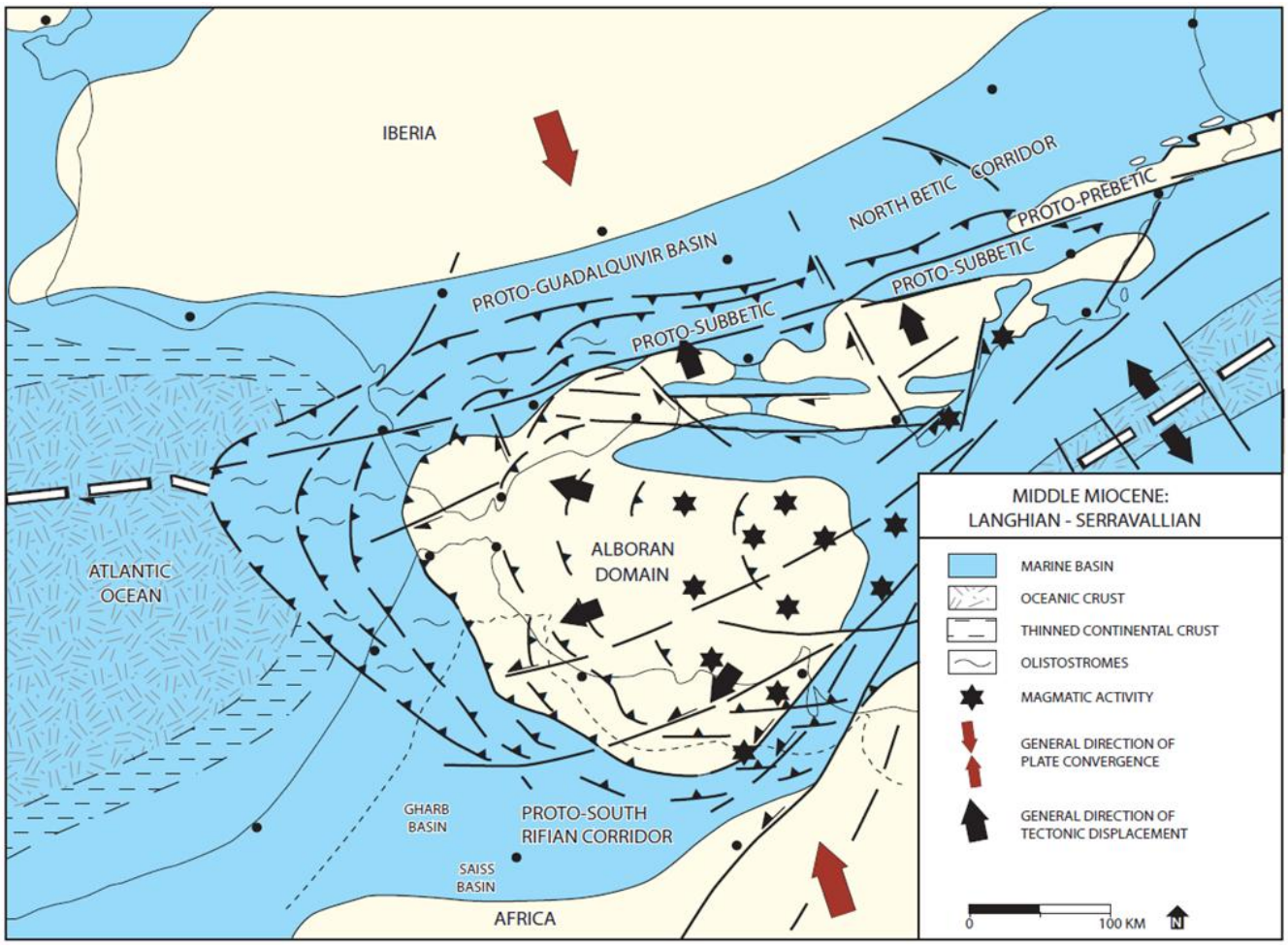

Figure 10: paleogeographic reconstruction for the Langhian-Serravallian (Sissingh et al., 2008). *The westward migration of the Alboran Domain results in the formation of two oceanic straits due to the existence of a foredeep surrounding the Domain.*

Comas et al. (1999) describe that when the lithospheric mantle is completely removed, the surface could be uplifted with an amount of 3000m maximum, depending on the initial thickness and composition. When convective removal is the mechanism responsible for removing lithospheric mantle material, 2000 to 3000m is defined as a maximum uplift (England & Houseman, 1989). Because it is not sure which process is responsible for the uplift in the region, I use a maximum height of 2000m. This height is used to calculate the associated forces due to potential energy difference in the Domain with respect to its surrounding lowland (see Table 1), according to the method of Molnar & Lyon-Caen (1988). The absolute height of the Domain in the past is not relevant, but by inducing a certain high, the difference in gravitational potential energy necessary for the gravitational collapse can be created in my model.

Table 1: Potential energy difference between crest maximum and surrounding lowland. Calculated according to the method of Molnar & Lyon-Caen (1988)*.*

Crest height (m)	Potential energy difference (Nm^{-1})
4000	$5.603472 * 10^{12}$
2000	$2.362248 * 10^{12}$
1000	$1.071252 * 10^{12}$
500	$5.081580 * 10^{11}$

The calculated potential energy difference of $1.07 * 10^{12}$ Nm^{-1} related to a height of 1000m is close to the magnitude of $1 * 10^{12}$ Nm^{-1} used for convergence and roll-back related pull. When the high is increased or decreased by a factor of 2, the associated values also resemble the minimum and maximum values of the convergence and pull. This is a good indicator that the correct height of the Alboran Domain is used in the model.

The potential energy contrast of $5.6 * 10^{12}$ Nm^{-1} associated with a crest height of 4000m (Table 1) is calculated to see what height is necessary in my model for resembling the GPE contrast per horizontal meter of contact of $5.1 * 10^{12}$ Nm^{-1} between the Alboran Domain and the continental margins calculated by Platt (2003). His calculation implies an Alboran Domain elevation of 4668m and an Iberia elevation of 683m, which is almost the same to my setup of 4000m and a surrounding lowland of 0m. The main difference between these two calculations are the changes in crustal and lithospheric thicknesses as well as density between the Alboran Domain and Iberia, but at first-order they show a good resemblance. This is another positive indicator that a chosen maximum crest height of 2000m during the Late Miocene is a realistic value, because the calculation of Platt (2007) is made to find the contrast between the Alboran and Iberia 19 Myr ago. Therefore it is plausible to say that the Alboran Domain lost around half of its gravitational potential energy during this time interval.

4.5 Eastern Pyrenees

The location of the super positioned high in the Eastern Pyrenees is based on the 2D-model results of Gunnell et al. (2008), where they show that a lithospheric root is missing east of 42.3°N 2.5°E. The highest amount of uplift will occur at the position where the original lithospheric root was thickest,

the axial zone, which is located at the same 42.3 degrees latitude, therefore this latitude is chosen as the position for my high. The top of my induced high will be at 3°E so that its main influence will be east of 2.5°E.

Because it is not sure how much of the lithospheric root is missing, and by which mechanism, the same amount of uplift is used as in the Alboran Domain with a maximum of 2000m, which agrees well with the maximum suggested by Gunnell et al. (2008). The authors calculate a maximum of 1700 to 2100 m uplift from the existence of peneplains at a high elevation in the Pyrenean orogen. The big difference with the Alboran Domain is the small contour surrounding the high of only 1 degree in radius, causing it to have a relative steep gradient. The Pyrenees are a narrow chain, so a small contour is chosen to see what the influence will be of a very local anomaly.

5. Results

All results are constructed in the order described by the matrix in Appendix D, but of course not all results can be displayed. The figures which are discussed in the following section are visible at the end of section 5. All figures shown are generated using the Generic Mapping Tool (GMT) (Wessel & Smith, 1991) and this section will start with the results relating to the Betic region. In all these results the continents in light-gray can be seen in the background with on top a contour defining the boundaries of the Alboran Domain. The thick black line represents that part of the contour which defines the uncoupled internal boundary. In the middle of the contour you can see a thin gray line which represents the crest of the Domain. Both the contour and crest line will be present in every result, even when the gravitational spreading due to the Alboran Domain is not active, to be able to compare the results better.

5.1 Betics

The three contributing forces will first be shown individually, to see how the stress-pattern responds to each force. It is important to show these: in this way we will be able to identify which force is controlling the stress field when it is subject to a combination of forces. Modeled stress magnitudes scale linearly, patterns in the stress field are not depend on the force magnitude. The individual forces shown here are the maximum magnitudes I used in my models.

5.1.1. Forces individually

Figure 11 shows the stress field obtained with only convergence with a magnitude of $2 * 10^{12}$ Nm^{-1}. The main observations are that the field is uniform to the NNW-SSE convergence, except for the area which is influenced by the uncoupled internal boundary to the west. The shape of this boundary causes the compression to be deflected and a “shadow zone” appears to the east of the boundary, where the convergence does not result in significant stresses. Some edge effects appear close to the northern termination of the internal boundary, the SW-NE tension visible is such a response only due to the shape of the boundary.

Figure 12 shows the stress field obtained with only roll-back related pull with a magnitude of $2 * 10^{12}$ Nm^{-1}. The pull is depicted by the long white arrows. General observations are a strong tensional

stress to the east of the internal boundary, but the tension diminishes fast towards the east. Close to the boundary, tension occurs also in north-south direction. There is almost no response to the west of the boundary, except for one relative large stress at the southern end of the internal boundary, which is probably an edge effect.

Compressional stresses to the west of the boundary are larger at the northern and southern part of the boundary, there is almost no compression in the middle: compression is not caused by the pull itself, but by the tensional stresses of the rest of the field, which are slightly curved around the internal boundary, causing compression in that part of the field.

Figure 13 shows the response of the field to the spreading forces originating in the Alboran Domain, which in this case has a crest height of 2000m. The associated forces have a maximum value of $2.36 * 10^{12}$ Nm^{-1} (Table 1). Tension develops near the crest, mainly perpendicular to the elongated WSW-ENE shape of the Domain, but also some parallel components appear. At some distance from the crest the tension is radial, especially to the north and south. The largest principal axes display a circular pattern at the rim of the Alboran Domain, while outside the contour the stresses are hardly of any influence. The uncoupled internal boundary does not seem to alter the pattern either.

A second colored version of model R64 is displayed (Fig. 14) to give an idea on how the topography is smoothened. The brightest brown colors are close to the maximum of 2000m, the darker it gets, the lower the elevation, until the lowest level of 0m. Be aware that the scale of the stress is different to the previous figure; the white contour is the same as the thin gray contour in the previous figure.

5.1.2. Combination of convergence and roll-back related pull

Now we will have a look at the combination of only convergence and roll-back related pull. If the ratio between the two forces remains the same, the orientation of the field will not change.

Figure 15 is the result of the combination of a westward pull and a NNW-SSE convergence both with a magnitude of $2 * 10^{12}$ Nm^{-1}. As you can see the convergence is the main factor controlling the stress pattern, while the westward pull only influences the area nearby the internal boundary. Even when the pull remains the same and the convergence decreases to a magnitude of $0.5 * 10^{12}$ Nm^{-1} as shown in figure 16, the stress due to the pull will not penetrate that far into the Alboran Domain. It does change the direction of the stresses caused by the convergence; which will bend around the internal boundary resulting in a NW-SE direction in Iberia, instead of an initial NNW-SSE direction (see Fig. 11).

5.1.3. Combination of gravitational spreading forces and convergence

Figure 17 displays the result of the stress field in response to an Alboran Domain with a height of 2000m in combination with convergence of $2 * 10^{12}$ Nm^{-1}. The compressional stresses can penetrate the Alboran Domain up to the crest, where the NNE-SSW tension balances with the compression in that same direction. Tension in a WSW-ENE orientation is maintained, the magnitude is even slightly increased when compared to the original field influenced by the Alboran Domain alone. And the orientation of tension is more parallel to each other than before.

The principal axes at the NE corner of the Alboran Domain are slightly deflected away from the high; this effect is even stronger when you look at figure 18, where the convergence is weakened to $1 * 10^{12}$ Nm^{-1}. NNE-SSW tension is visible again at the crest due to this weakening. When the convergence is weakened even more, the stress field (Fig. 19) resembles the original field (Fig. 13) and the convergent force has only influence on the area outside the contour of the Alboran Domain.

5.1.4. Combination of gravitational spreading forces and roll-back related pull

When the Alboran Domain of 2000m is combined with a roll-back related pull of $2 * 10^{12}$ Nm^{-1} the principal axes start to rotate as if the plate is sucked into the zone where the pull is most effective, see figure 20. The tension which originally was oriented perpendicular to the crest is now turned parallel to the crest.

If the pull is kept constant, but the height of the Alboran Domain decreases to only 500m with an associated maximum force of $5.1 * 10^{11}$ Nm^{-1}, the response of the stress field (Fig. 21) resembles that due to the original pull (Fig. 12). Tension is now only present in the direction of the pull, except for stresses very close to the internal boundary. The magnitude of the tension is increased compared to that of the original model R4 (Fig. 12), especially along the crest.

The other extreme scenario is a combination of an Alboran Domain of 2000m with a relative weak pull of only $0.5 * 10^{12}$ Nm^{-1} (Fig. 22). Again, the response of the stress field is quite similar to the original field response due to the gravitational spreading forces only (Fig.13). The only differences are some small rotations when getting close to the internal boundary.

5.1.5. Combining all three involved tectonic forces

I cannot show all modeled combinations but I will start with the general field where all forces have their maximum magnitude: an Alboran Domain of 2000m, a westward roll-back related pull and a north-south convergence of $2 * 10^{12}$ Nm^{-1}, figure 23. The response of the stress field shows some resemblance with the fields where only two forces are combined. The convergence balances with the Alboran Domain, compressional stresses intrude at the rims of the Domain and remain strong up to the crest where the original tensional forces induced by the Domain are completely compensated and not visibly anymore. Tension now remains only in WSW-ENE direction due to the combined effect of the pull and the existence of the Alboran Domain. The field shows a little deflection in the NE also.

Next we will consider three model results which could resemble the broad geological evolution in the area, just prior to, during and after the Messinian Salinity Crisis. In the discussion the choice for this models will be explained.

1) Figure 24 show the field response to a moderate Alboran Domain (1000m), and both convergence and roll-back related pull with a magnitude of $1 * 10^{12}$ Nm^{-1}. The response of the stress field is the same as the previously described field R49 (Fig. 23), only the magnitudes are decreased.

2) Figure 25 shows the stage where the roll-back related pull has completely come to a halt, the height of the Alboran Domain is decreased by a factor of 2, while the magnitude of convergence remains the same. When the convergent force is dominant, the stress field will overprint any influence of the Alboran Domain. The only visible remainder is a reduction in compression at the crest and a very limited tension in a WSW-ENE direction.

3) In figure 26 the height of the Alboran Domain is decreased to a minimum of 0m and has no influence on the field anymore. The convergence remains constant, and the roll-back related pull reactivates, although weaker than before. The convergence is the controlling force; the weak pull has only influence on the region very close to the internal boundary.

5.2 Eastern Pyrenees

A small side-step to the Eastern Pyrenees is made because I can apply a similar method, the combination of a potential high with a converging stress field, to obtain some results. First I will show the response of the stress field to the gravitational potential high only, before I combine them with convergence.

5.2.1. No convergence

Figure 27 shows the response to a gravitational potential high which is simulated with a top of 1000m. The contour is circular, so the stress-pattern is circular as well. It may seem to be a bit elliptical, north-south direction is extended with respect to east-west direction. This becomes even more clear in the results with convergence, where the contour lines of the high are plotted. In this figure this is not displayed because the position of the high with respect to the land margin in the background is important. The mesh is visible to identify the boundaries of the finer mesh.

There is radial tension at the top of the high, while principal axes display a circular pattern around the high perpendicular to the direction at higher elevation, which decreases in magnitude when moving away from the top. Similar behavior is visible in the Alboran Domain when receding from the crest (Fig. 13).

Figure 28 is similar to figure 27, only this time the high has a height of 2000m. There is no change in orientation, only the magnitude is increased. In this figure it looks like tension in east-west direction is stronger than in north-south direction.

5.2.2. Adding convergence

In the next two results the contour of the high is shown to let the part stand out which is mainly influenced by both components.

In figure 29 the high has the same height of 1000m as in figure 27, but now a convergence component of $1 * 10^{12}$ Nm^{-1} is added. The main effect is that the stresses visible in figure 27 rotate anti-clockwise by ~ 20 degrees. Tension is still present, but now only in a NE-SW orientation. Compressional forces penetrate the high at the boundaries, and are strong enough to overcome the force induced by the highest point in a NW-SE direction. The field outside the contour is practically not influenced by the high, because it had such a small effect in the first place (Fig. 27).

Figure 30 shows the stress field when the convergence remains constant at $1 * 10^{12}$ Nm^{-1}but the height is increased to 2000m. The stresses rotate in a similar fashion as in figure 29, especially close to the top. At the boundaries the principal axes of the stress originally responding to the convergence start to rotate into and deflect out of the contour. Due to the increase in height the outward tensional stresses become stronger, resulting in an almost balanced NNW-SSE compression/tension at the top.

Compression is still in control in this direction, while the tension in WSW-ENE is becoming even stronger. Not only on the inside of the contour of the high, but now also on the outside is the orientation of the field altered due to increase in height.

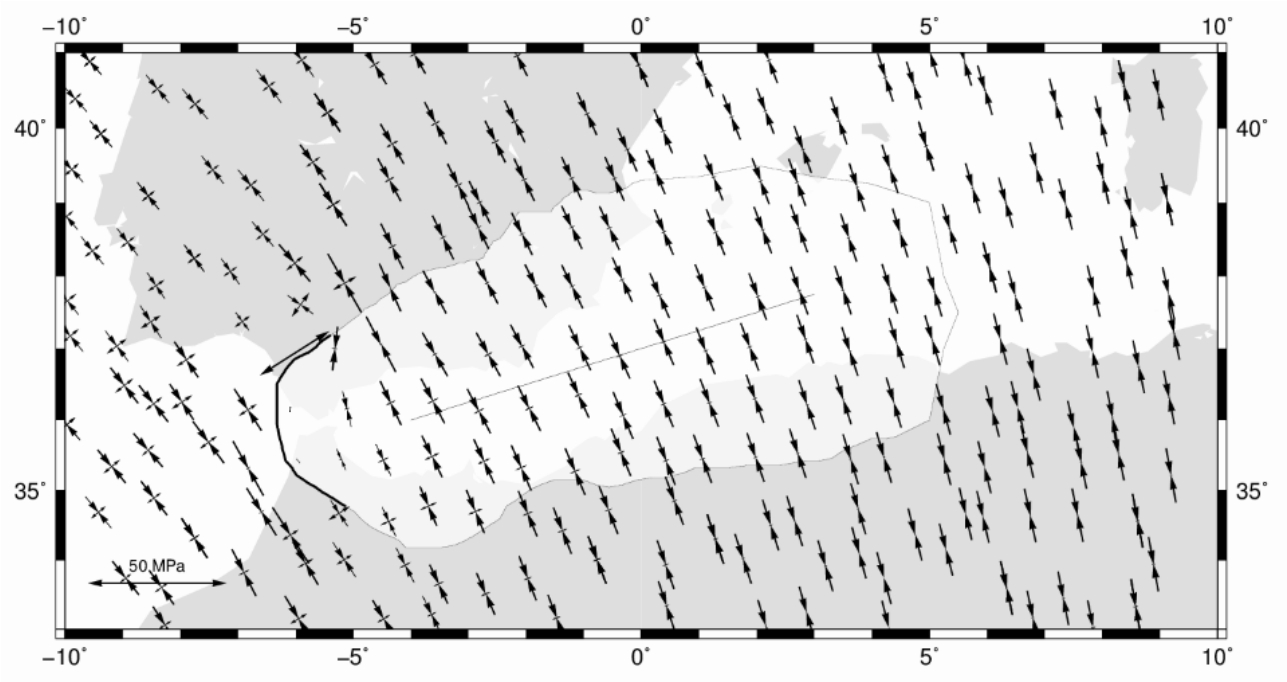

*Figure 11: Model R13, only convergence of 2 * 10^{12} Nm^{-1}.*

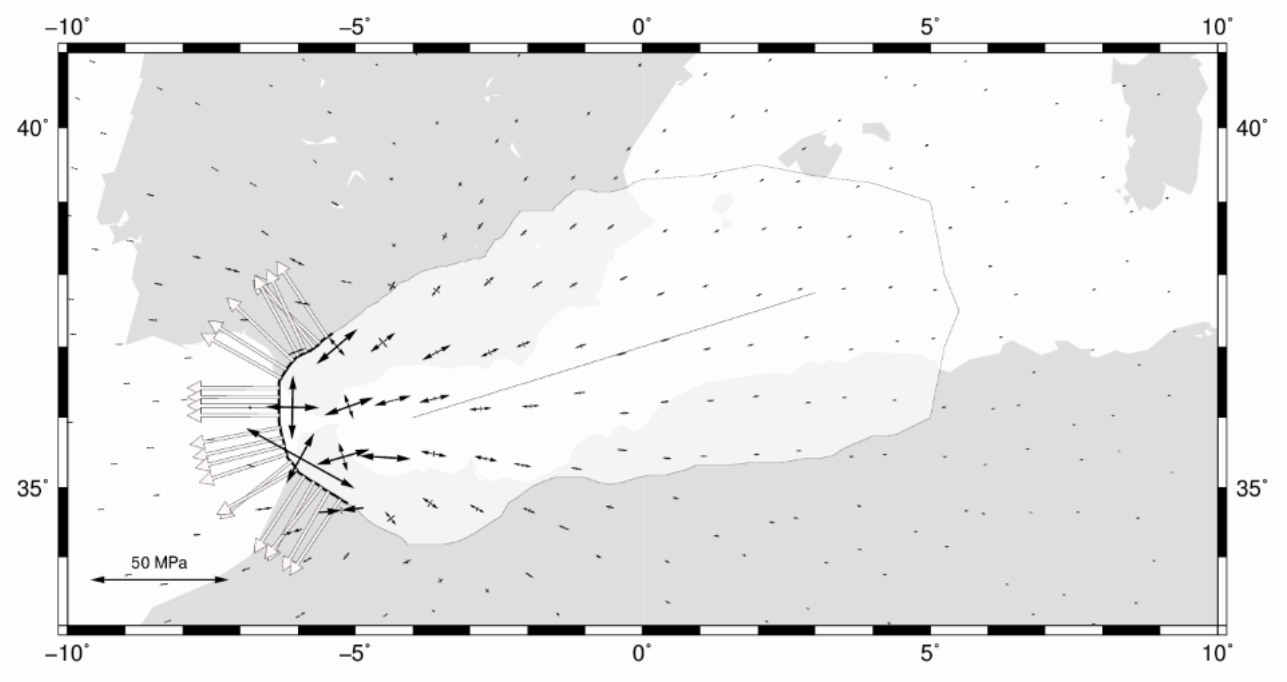

*Figure 12: Model R4, only westward pull of 2 * 10^{12} Nm^{-1}.*

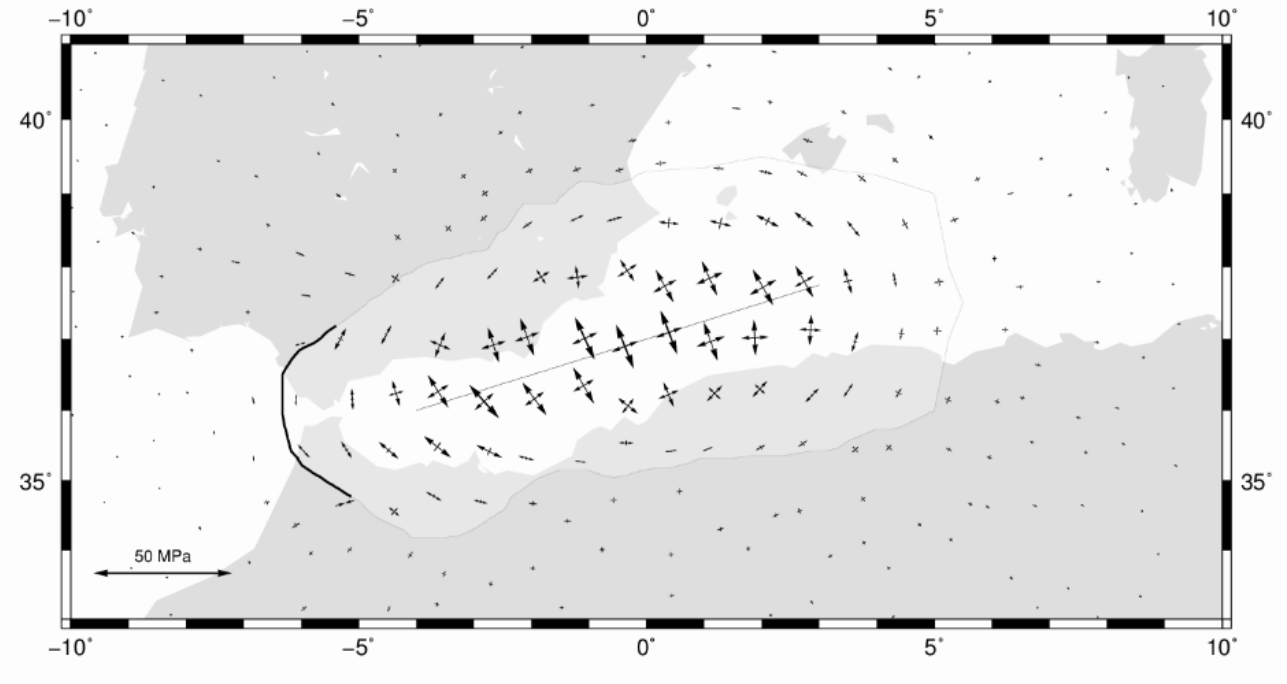

Figure 13: Model R64, only Alboran Domain with a crest height of 2000m.

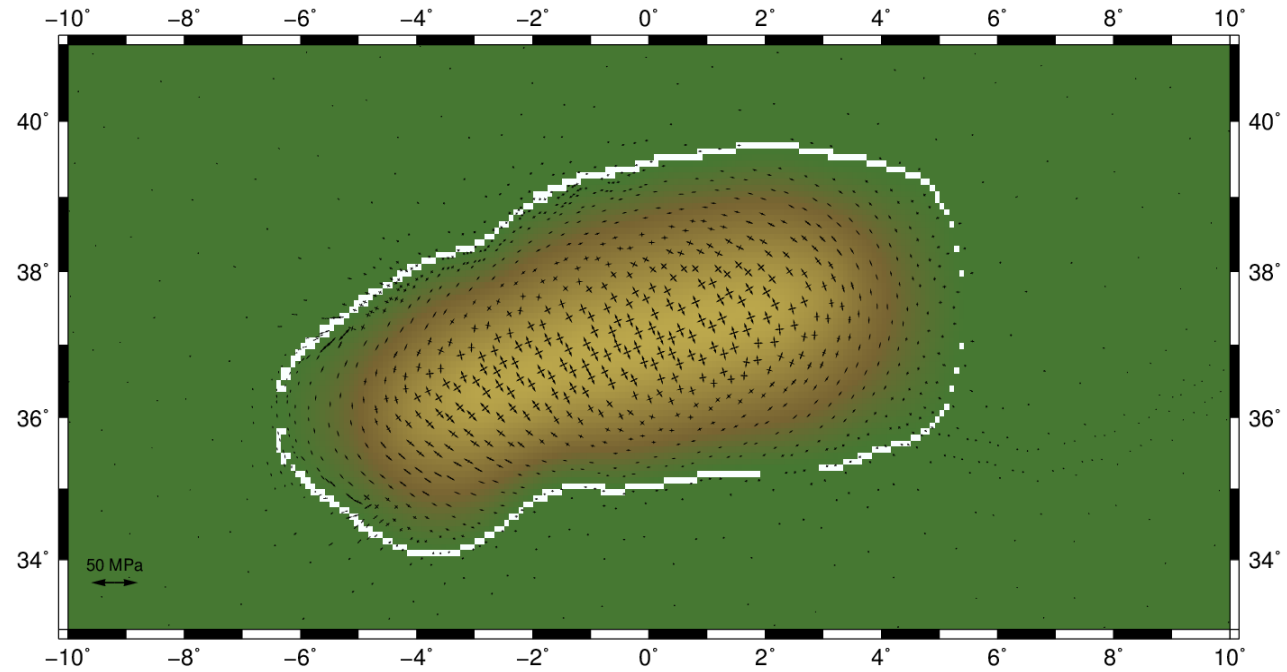

Figure 14: Model R64 again, different scale, and plotted more arrows. Just once to show the topography: yellow is highest (2000m max), green is zero.

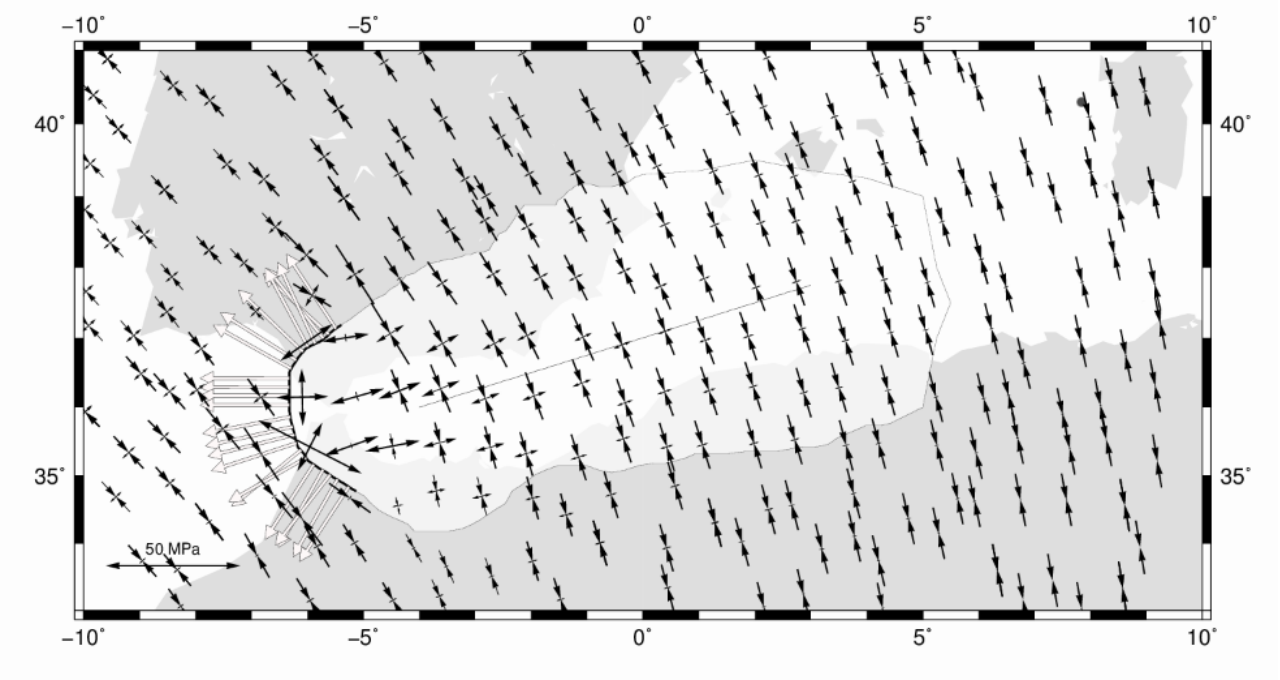

*Figure 15: Model R1, pull & convergence of 2 * 10^{12} Nm^{-1}.*

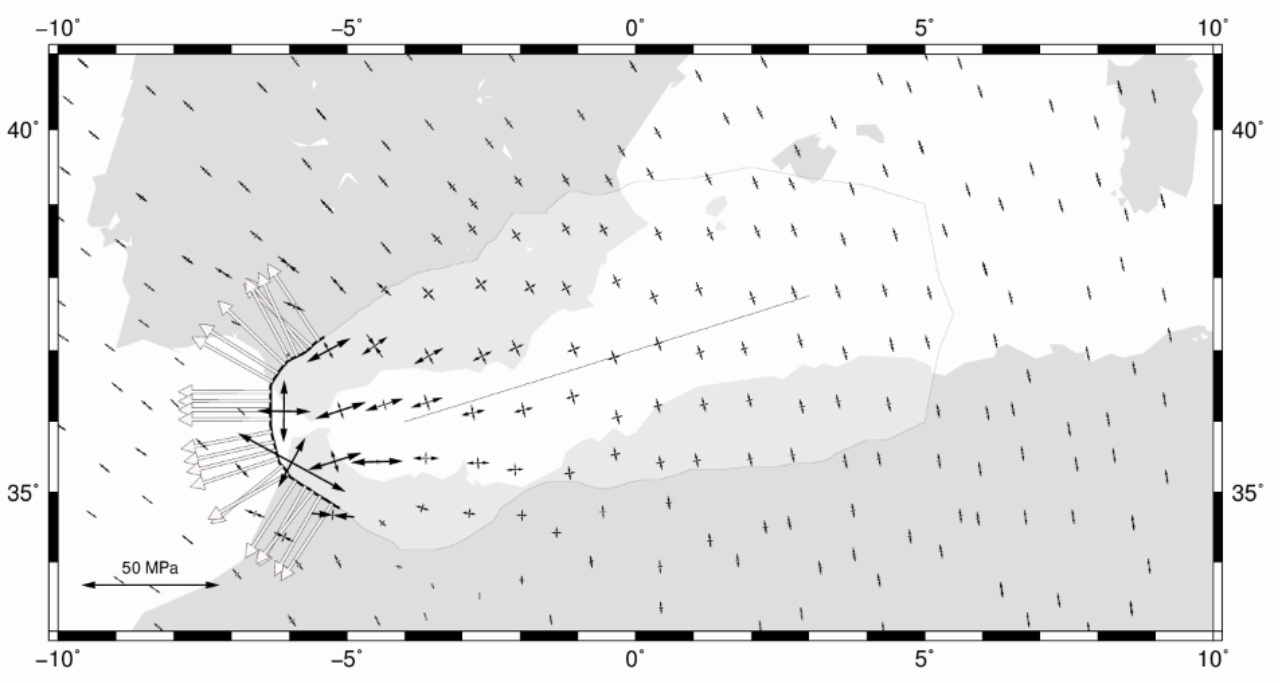

*Figure 16: Model R3, pull of 2 * 10^{12} Nm^{-1}, convergence of 0.5 * 10^{12} Nm^{-1}.*

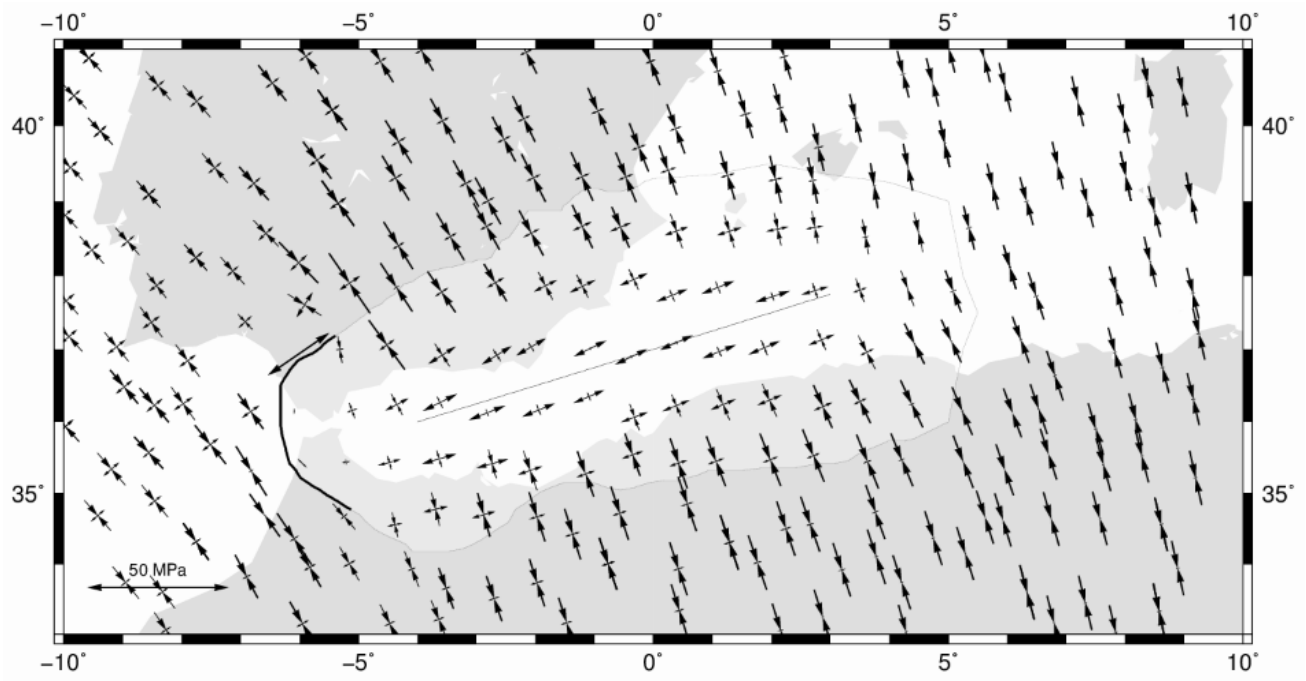

*Figure 17: Model R61, Alboran Domain of 2000m in combination with a convergence of 2 * 10^{12} Nm^{-1}.*

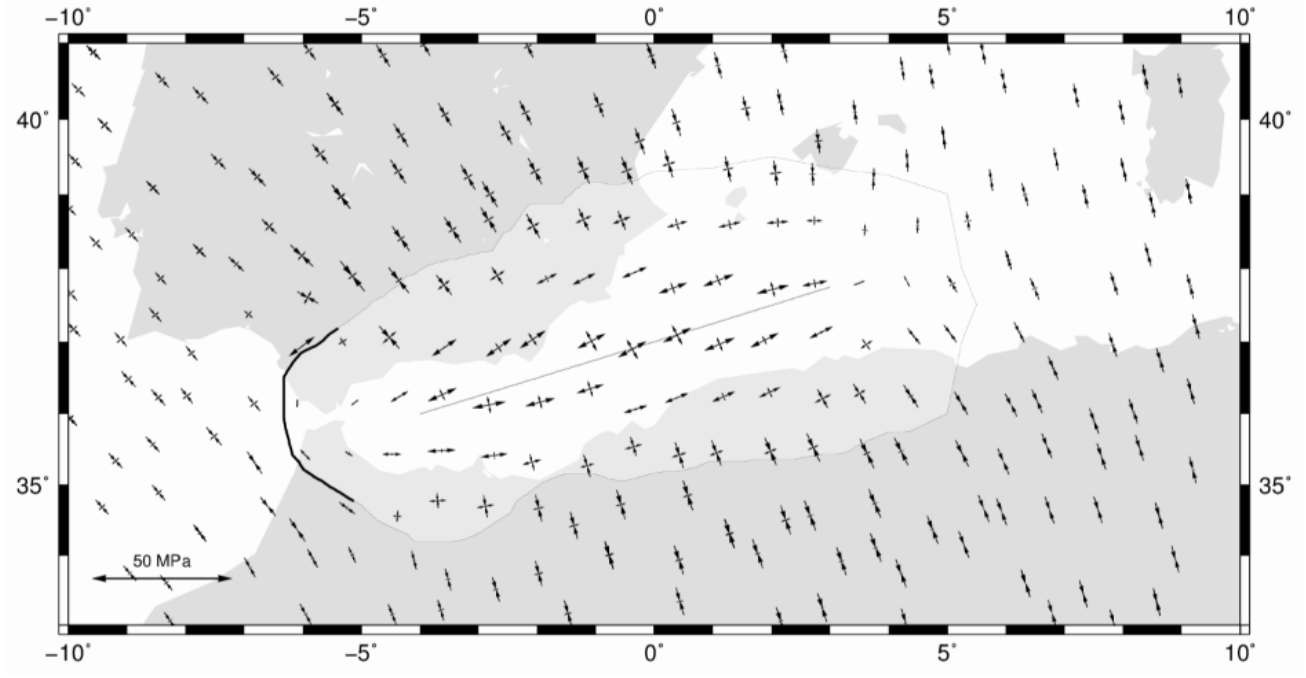

*Figure 18: Model R62, Alboran Domain of 2000m in combination with a convergence of 1 * 10^{12} Nm^{-1}. Normal faulting occurs at the crest as well as relative strong extension in SW-NE direction. Deflection NE corner of the field visible.*

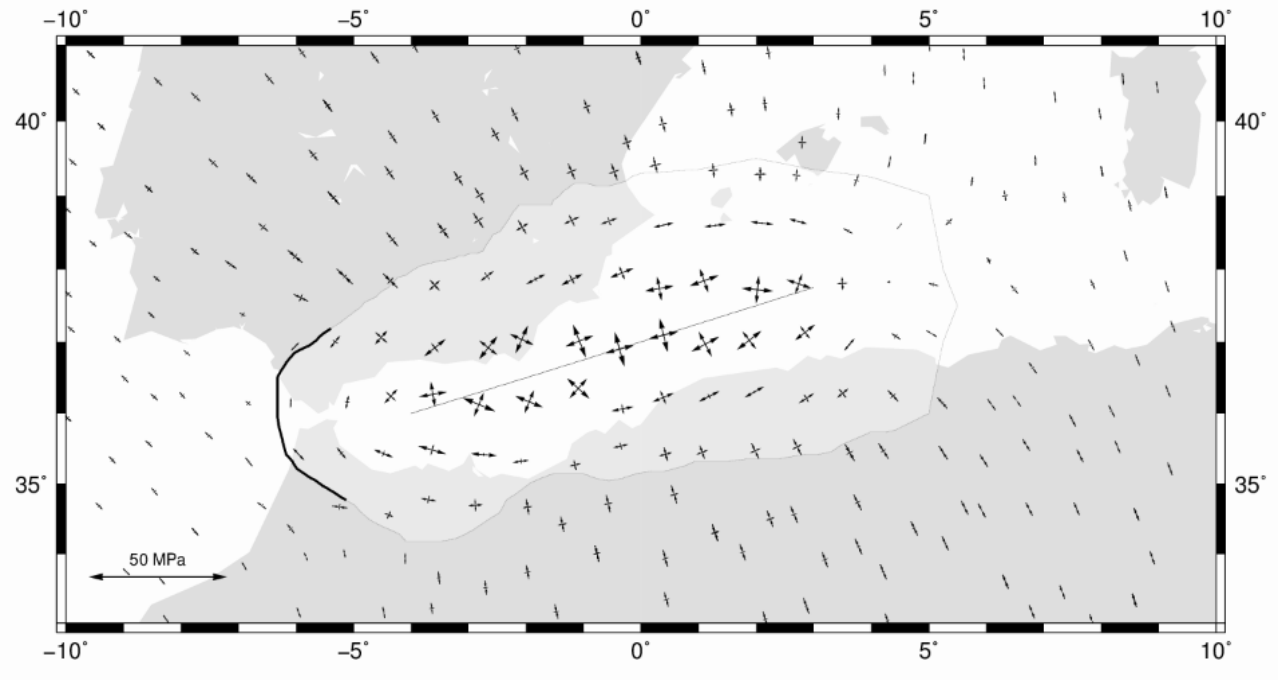

*Figure 19: Model R63, Alboran Domain of 2000m in combination with convergence of 0.5 * 10^{12} Nm^{-1}.*

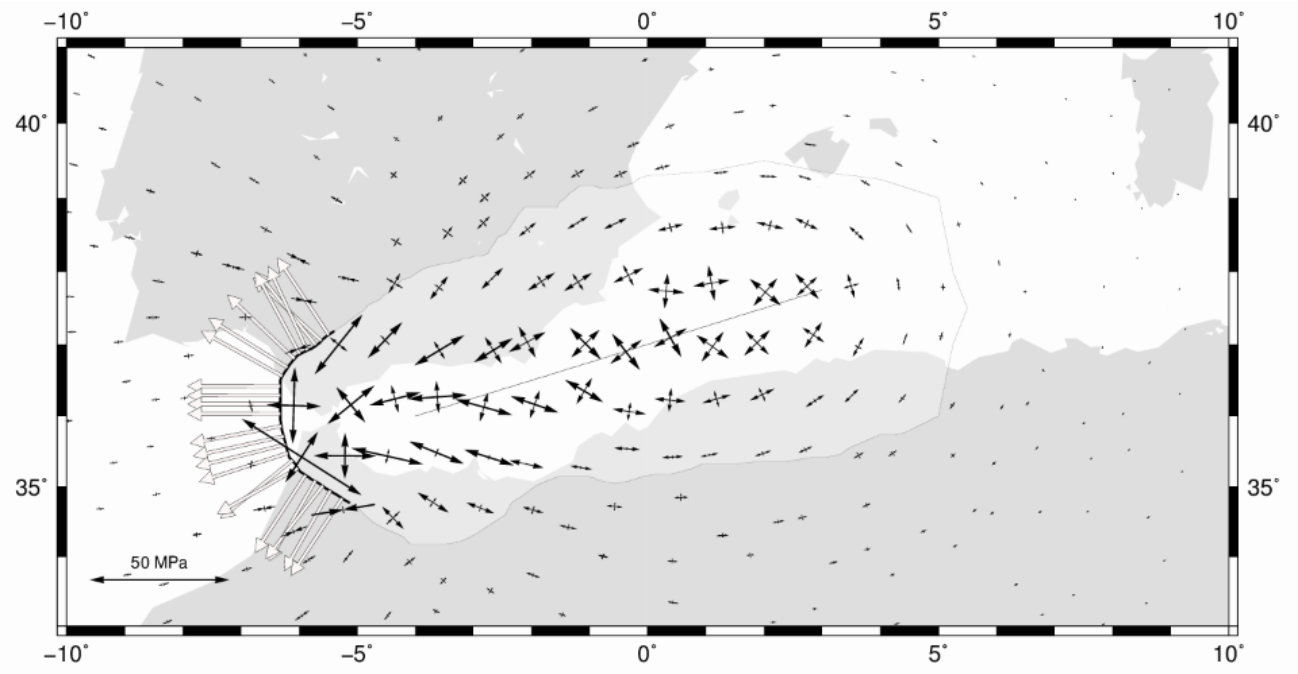

*Figure 20: Model R52, Alboran Domain of 2000m in combination with a pull of 2 * 10^{12} Nm^{-1}.*

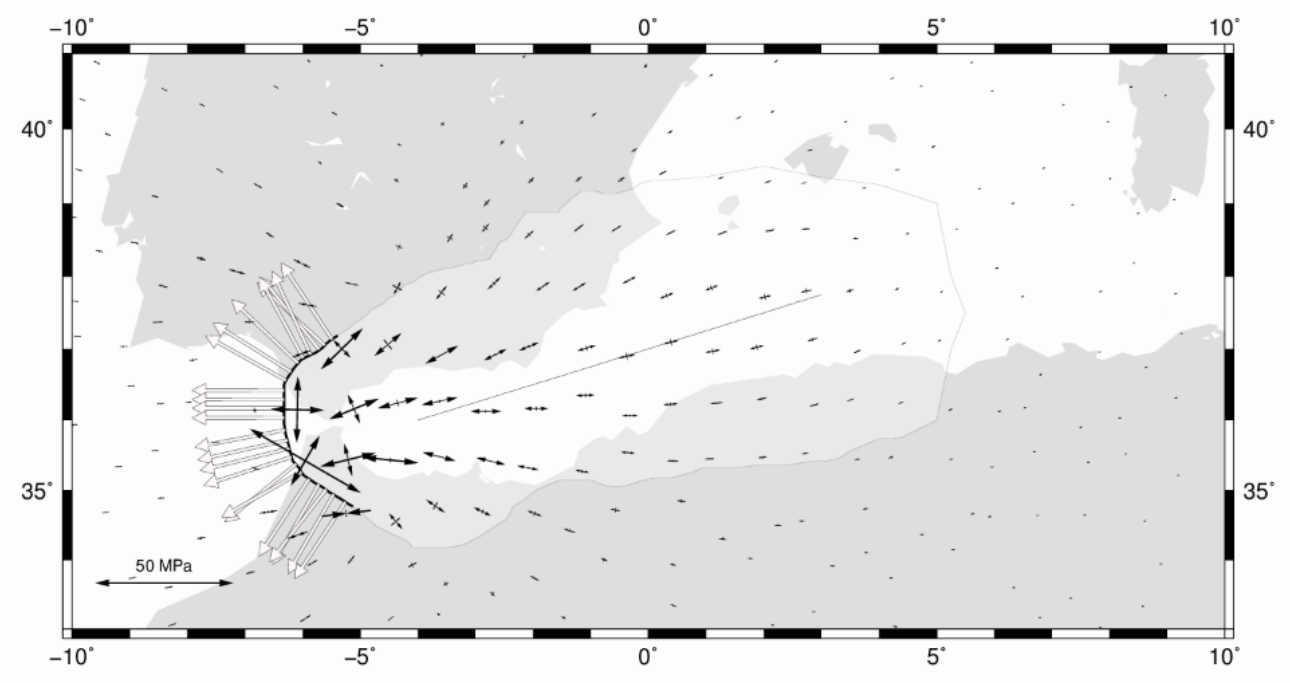

*Figure 21: Model R20, Alboran Domain of 500m in combination with a pull of 2 * 10^{12} Nm^{-1}.*

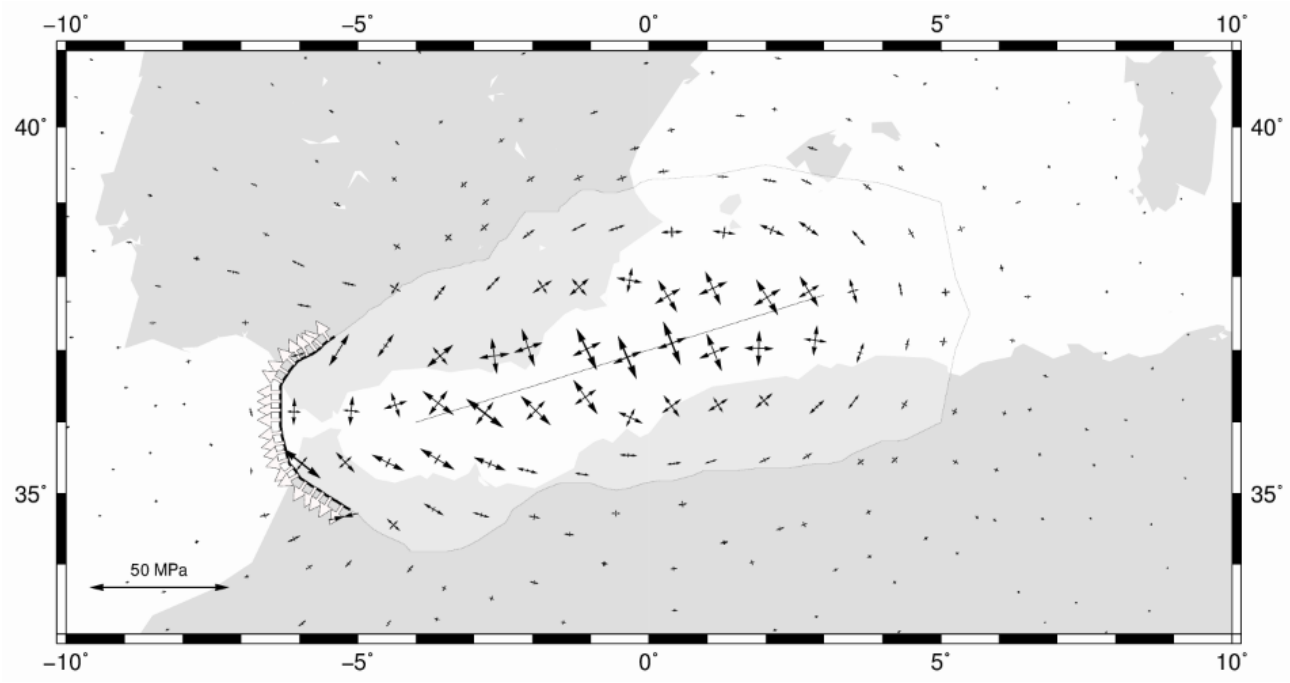

*Figure 22: Model R60, Alboran Domain of 2000m in combination with a pull of 0.5 * 10^{12} Nm^{-1}.*

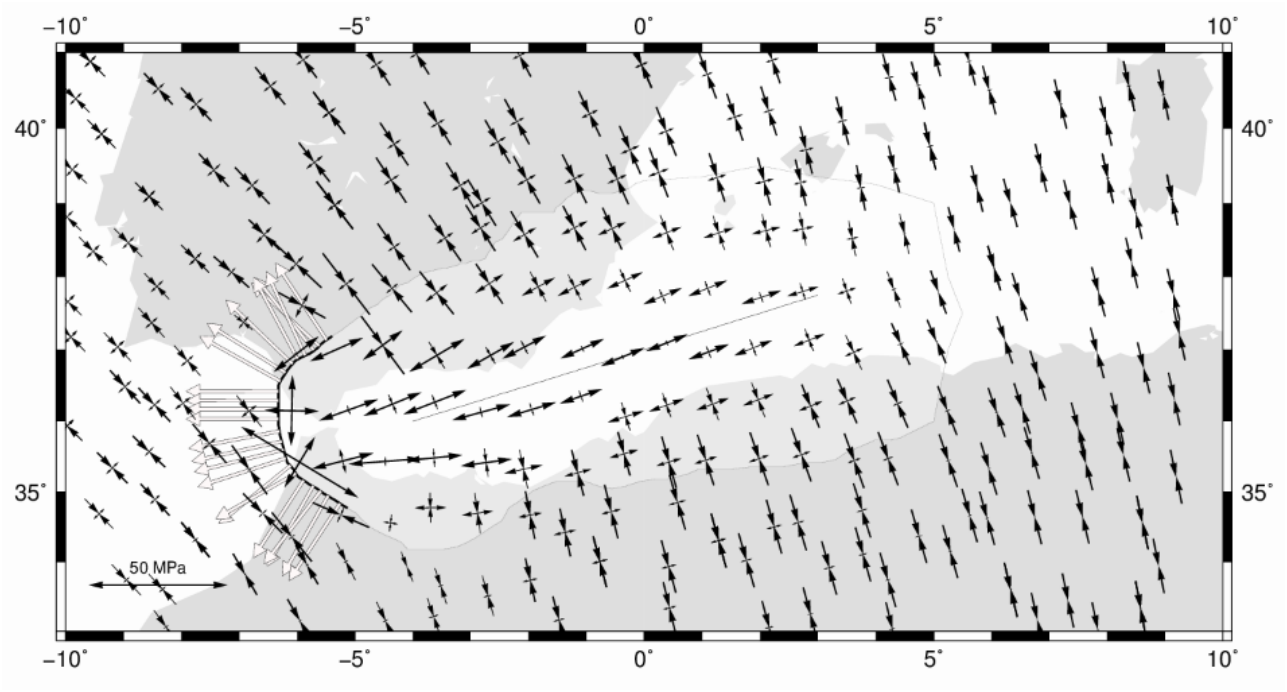

*Figure 23: Model R49, Alboran Domain of 2000m with a convergence and pull of 2 * 10^{12} Nm^{-1}.*

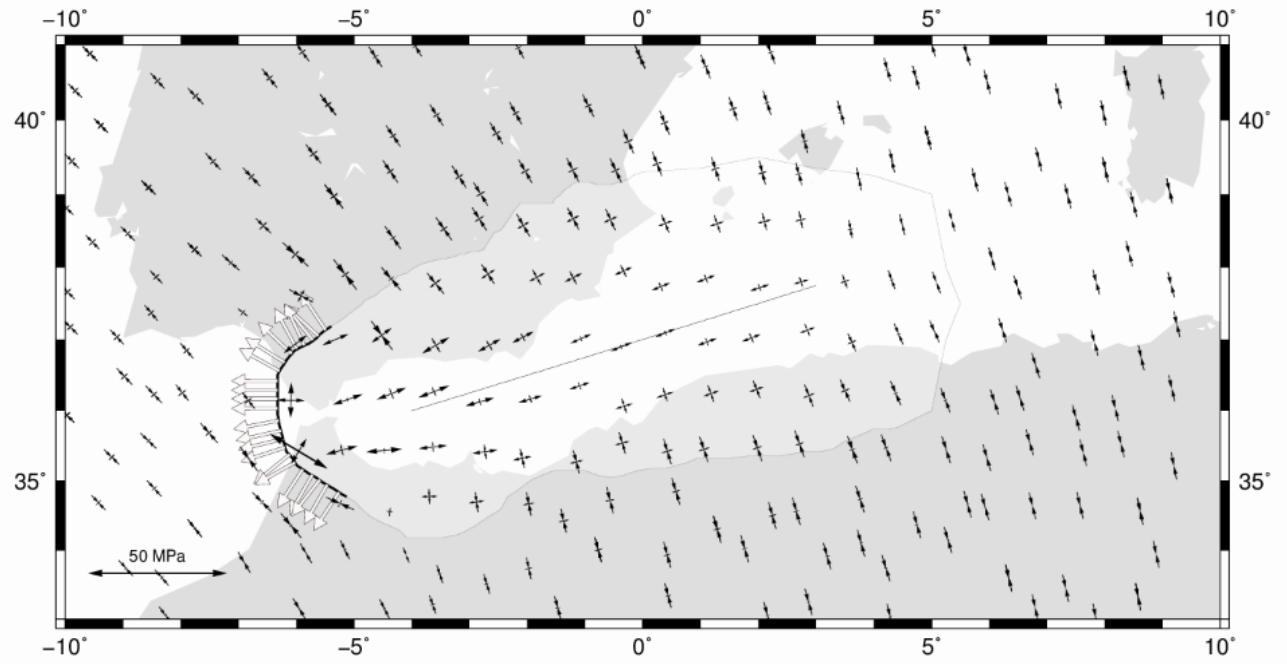

*Figure 24: Model R38, stage I of evolution, Alboran Domain of 1000m with a convergence and pull of 1 * 10^{12} Nm^{-1}.*

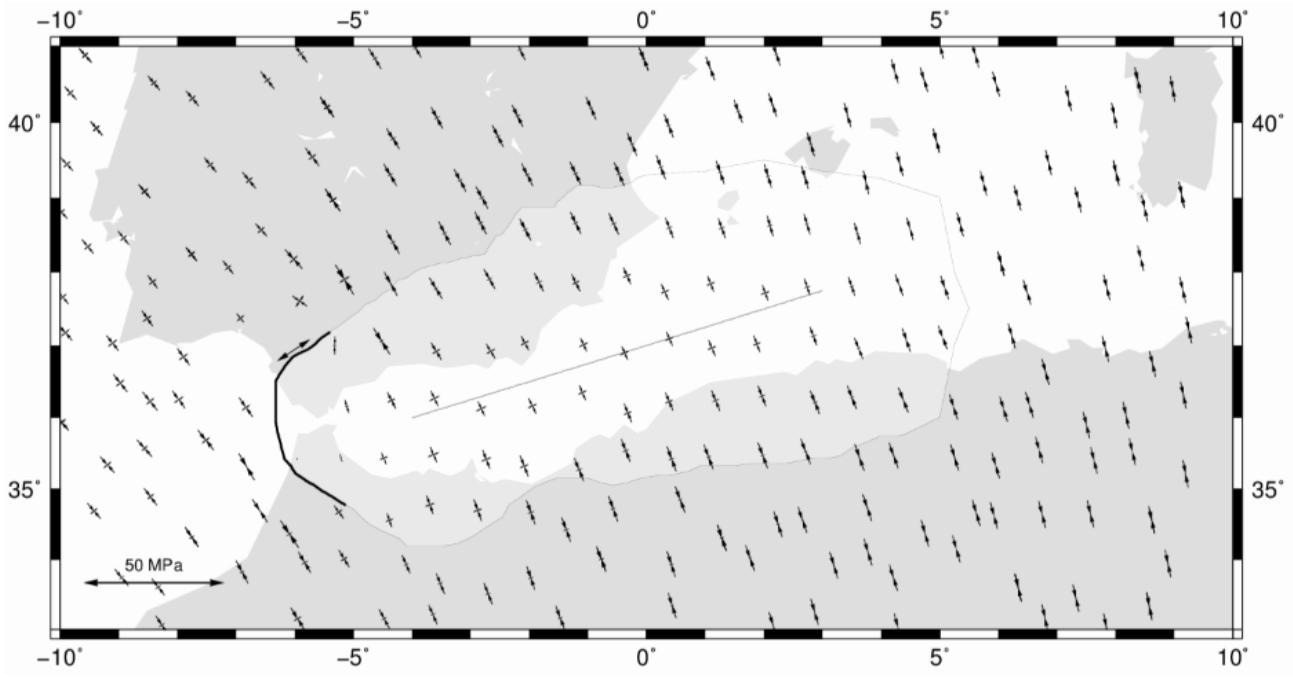

Figure 25: Model R30, stage II of evolution, Alboran Domain of 500m with a convergence of 1 10^{12} Nm^{-1}.*

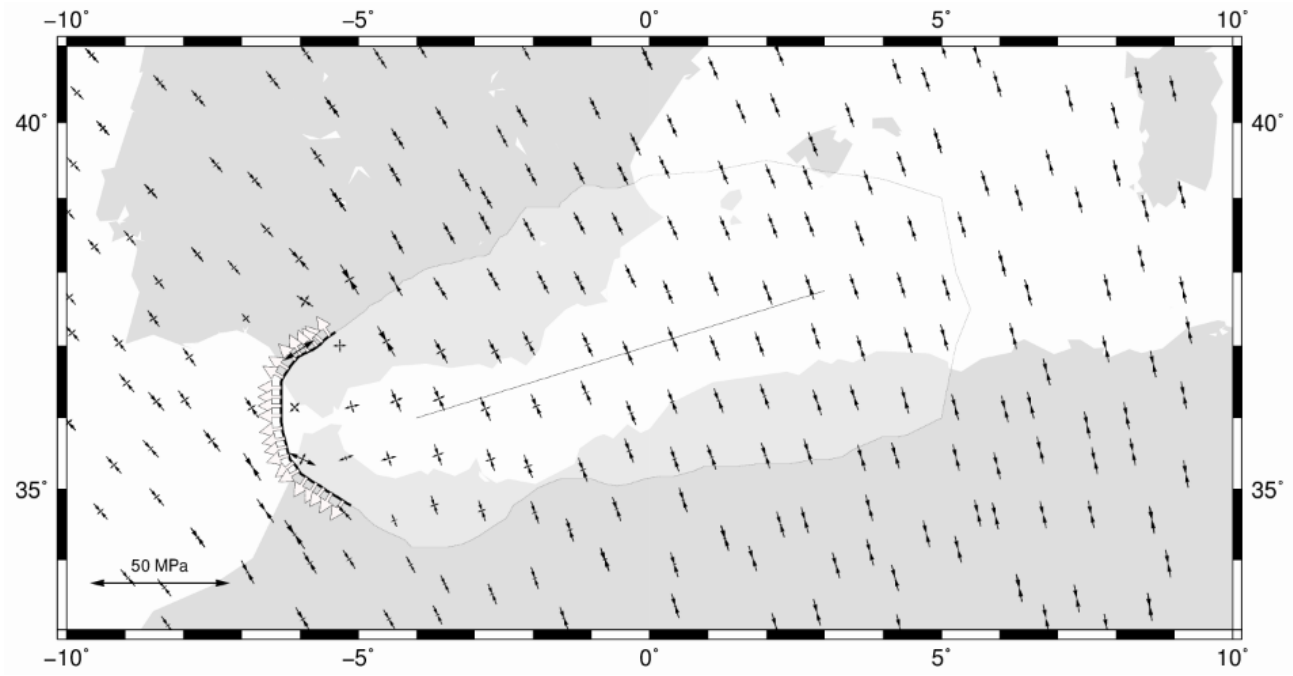

*Figure 26: Model R10, stage III of evolution, westward pull of 0.5 * 10^{12} Nm^{-1}in combination with convergence of 1 * 10^{12} Nm^{-1}.*

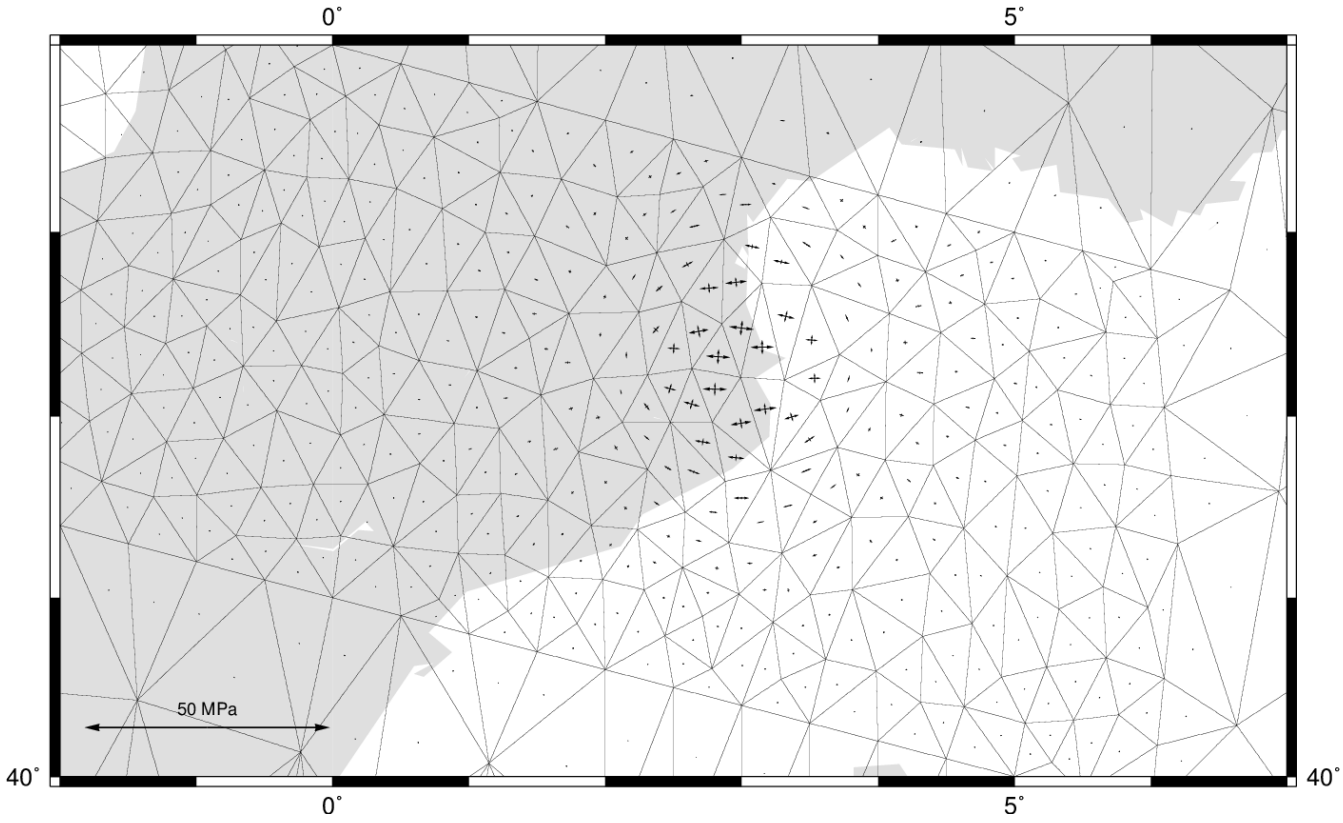

Figure 27: Model P1, height of top is 1000m.

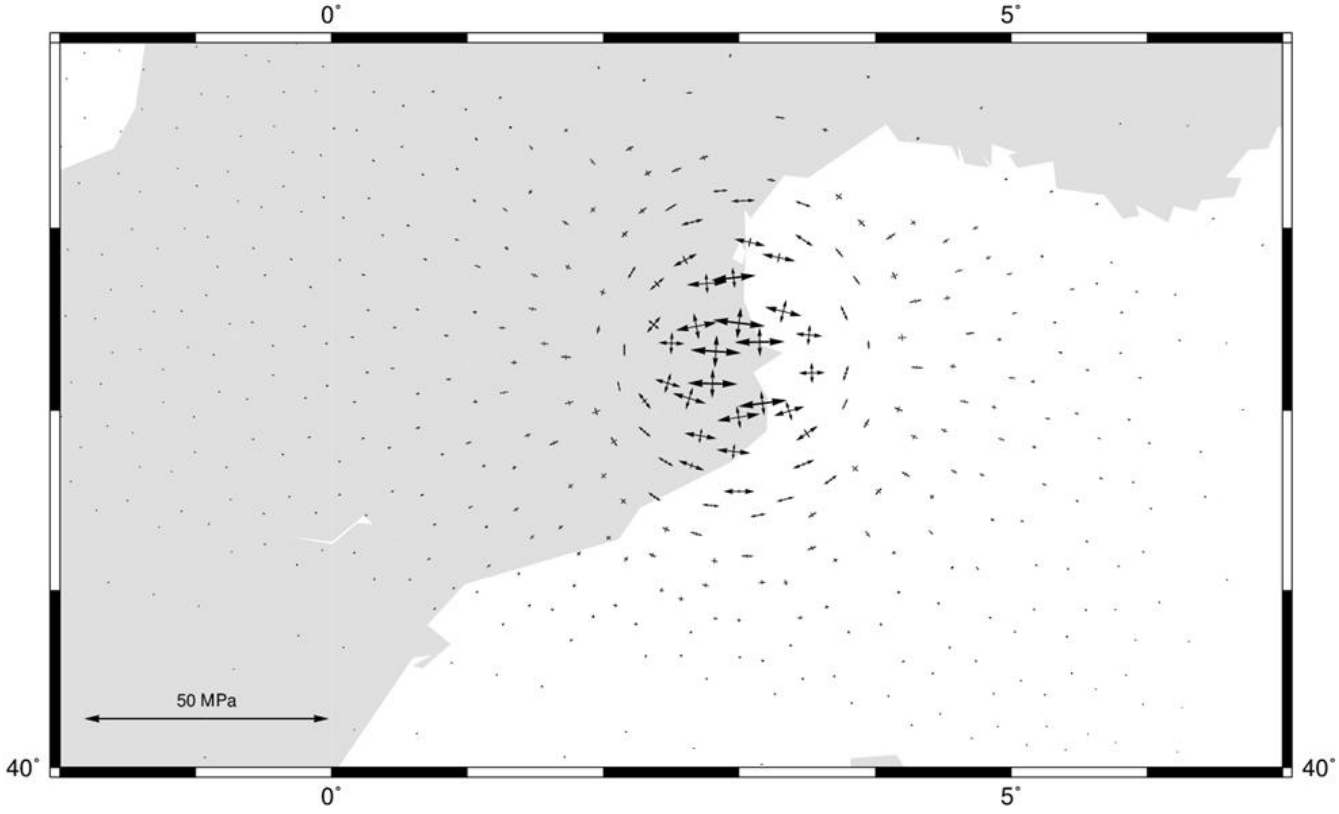

Figure 28: Model P3, height of top is 2000m.

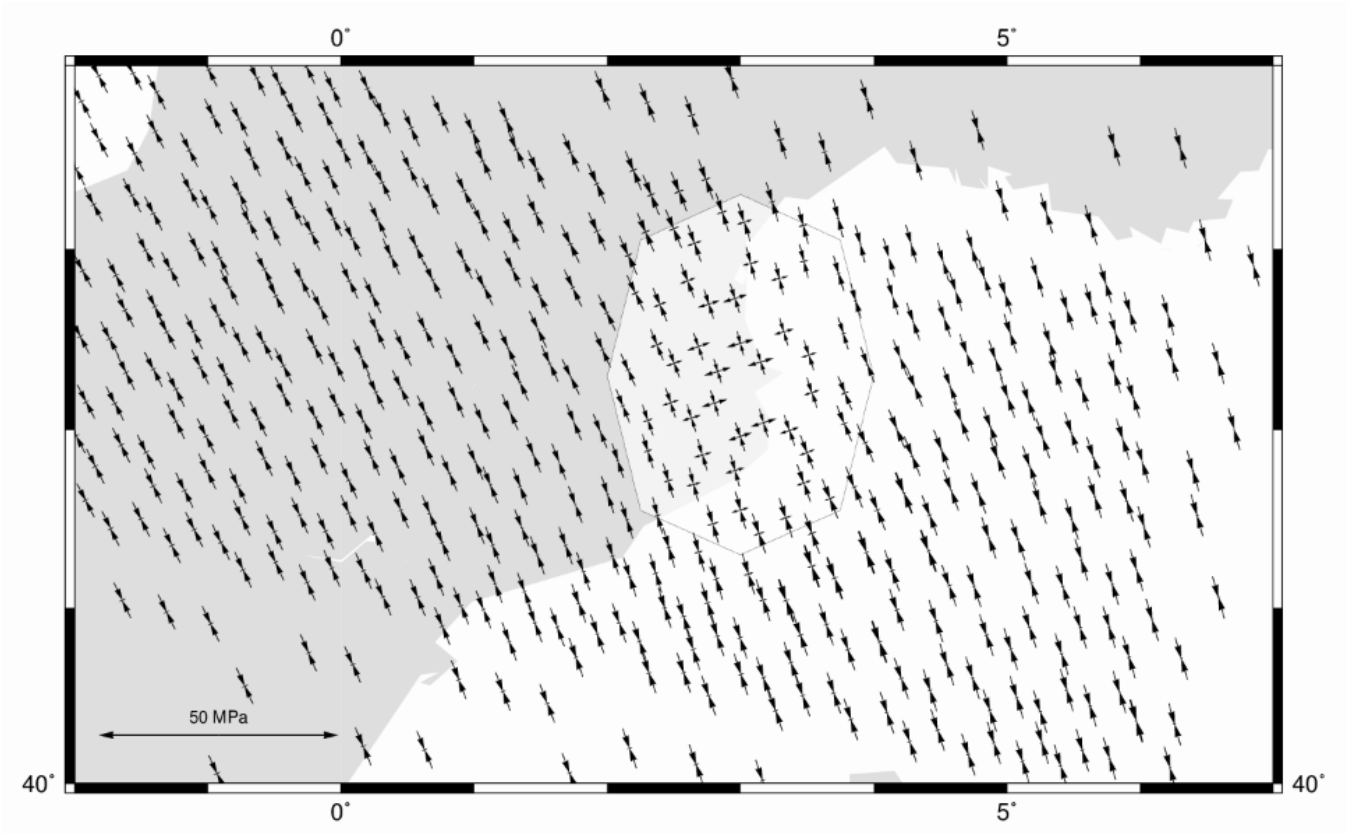

*Figure 29: Model P2, 1000m high in combination with a convergence of 1 * 10^{12} Nm^{-1}.*

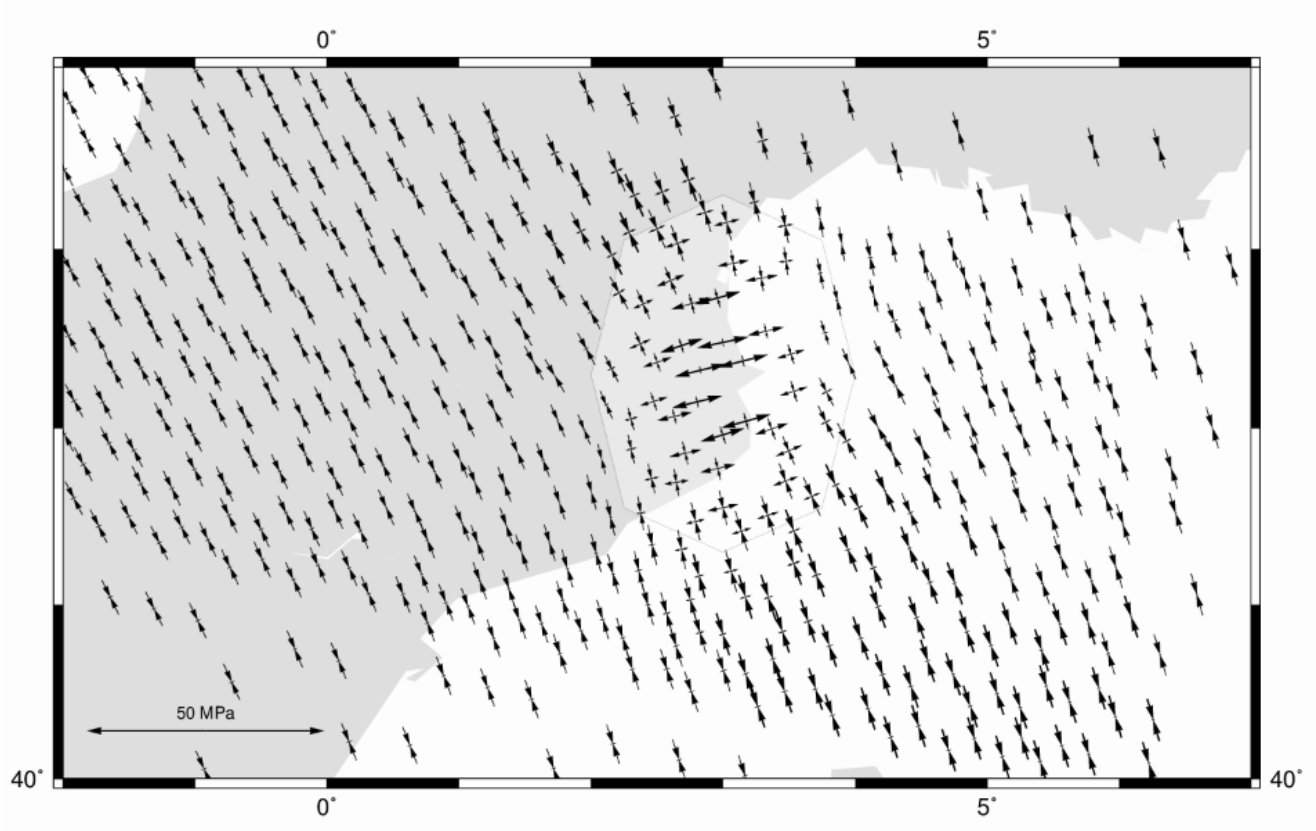

*Figure 30: Model P4, 2000m high in combination with a convergence of 1 * 10^{12} Nm^{-1}*

6. Discussion

6.1 Betics

6.1.1. Forces individually

Each response of the stress field to the three individual contributing forces, shown in paragraph 5.1.1., has a very distinctive character. The first two have some small edge effects near the internal boundary. When changing the shape of this boundary the edge effects shift, as can be seen in Appendix C. In figure 12 it is visible that the principal axes rotate around the uncoupled boundary, although the roll-back related pull should not have an effect to the west of this boundary. The element with a relatively large stress at the southern termination of the internal boundary indicates this rotation from east to west. Because the arc is so tight, the roll-back related pull on the northern side in combination with that on the southern side enhances the tension. This effect only plays a role close to the boundary, and has less effect on the rest of the field.

The high introduced to represent the increased gravitational potential energy shows normal faulting at the crest. The geographical location of this crest is positioned in the middle of the Alboran Sea, which is characterized by low-angle intracrustal detachments and shallow normal faulting (see Fig. 2) induced by Early to early Late Miocene extension (Sissingh et al., 2008). This is confirmed by Comas et al. (1999) who relate this faulting to Miocene crustal thinning, and Vissers (2012) who describes that cooling ages of associated mylonites indicate that these detachments were active during the early to middle Miocene. The WSW-ENE orientation of most of the normal faults present in the Alboran Sea agree well with the orientation of tension developed in the model due to gravitational collapse. As can be seen in figure 2, the orientation starts to change when approaching the Gibraltar Strait which can be related to the influence of roll-back related pull in the area.

The transition from tension at the crest to compression outside the contour makes sense; this compression could be expressed by the thrust faults observed in the Betics. This thrusting in the surrounding Betic & Rifian mountain belt was active coevally with extension in the basin according to Comas et al. (1999). The observed thrust faults have a predominant orientation of WSW-ENE (Sissingh et al., 2008) which agrees well with the direction of compression in the model.

The zone between the crest and the margins displays tensional stresses with an orientation perpendicular to the tension at the crest. This is caused by the gravitational collapse as well.
The SW-NE orientation of this tension would be consistent with the sinistral strike-slip transform faults bounding the extensional basins present in the internal zone of the Betics in the south-east of the Iberian peninsula, although Meijninger & Vissers (2006) show that during the Late Miocene, parts of the Alhama de Murcia fault (one of these sinistral faults) initiated as extensional normal faults as well.

A similar SW-NE orientation can be seen in the orientation of the Internal External Zone Boundary (IEZB). The IEZB was mainly active during Burdigalian time, it accommodated the westward motion of the AD and emplaced it onto the Iberian margin to the north. During the Middle to Late Miocene, further westward motion was accommodated on thrusts within the external thrust belt (Platt et al., 2013). My interpretation is therefore that the strike-slip faults present in the internal zone can be related to tensional stresses within the Alboran Domain and less to the westward motion of the Domain itself.

There are also major strike-slip faults present in Alboran Sea (Comas et al., 1999) which can be seen in figure 2 as well. The left slip in the south and the right slip in the north are indicators of the westward motion of the Alboran Domain, as described and shown in figure 31 (Platt et al., 2013).

Due to this westward motion, vertical-axis rotation occurs in a clockwise sense in the north, resulting in dextral strike-slip faults and in an anti-clockwise sense in the south resulting in sinistral strike-slip faults. According to Sissingh et al. (2008) this westward motion of the Alboran Domain had virtually come to an end around the Middle Miocene.

In the modeled stress fields, the higher amount of tension in SW-NE direction relative to that in NW-SE direction is caused by the elongated shape of the Alboran Domain. A more circular shape, as in the Eastern Pyrenees (Fig. 28), would have minimized this difference.

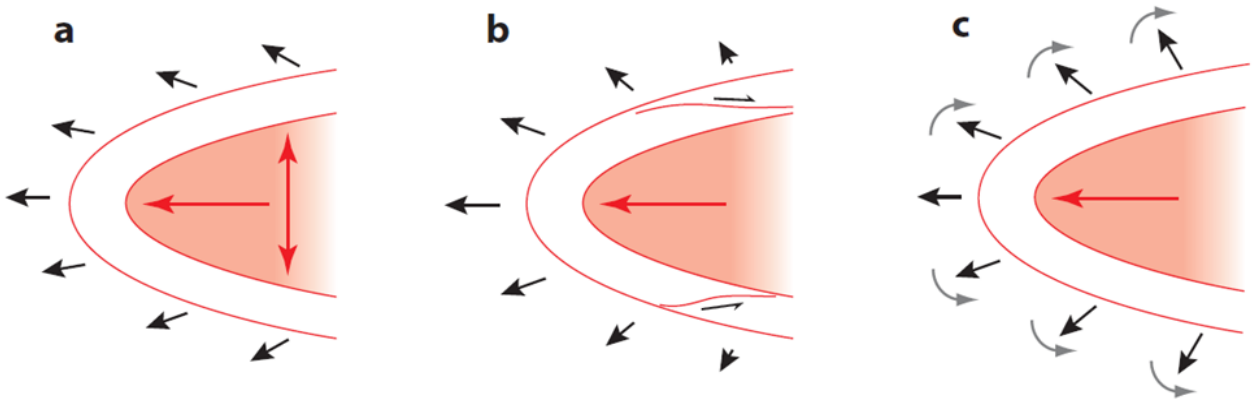

Figure 31: Explanations for the variation in transport direction in an arcuate thrust belt surrounding a moving hinterland region (Platt et al., 2013)*. Figure b shows the origination of dextral strike-slip faults north of the Domain and sinistral strike-slip faults south of the Domain. As long as the westward motion of the hinterland region is caused by a force along its axis, the northern and southern parts will be slowed down, causing vertical-axis rotation in a clockwise and anti-clockwise sense respectively (Fig. c).*

6.1.2. Combination of convergence and roll-back related pull

The combination of roll-back related pull and convergence (results 5.1.2.) shows that the field is most vulnerable to the convergence, because the stress induced by the pull does not reach that far into the domain. This makes perfect sense when looking at the individual forces: only a small part of the roll-back related pull is orientated perpendicular to the orientation of convergence, and only this part of the forcing can affect the level of stress penetration into the domain if a convergence related push of the same magnitude is active. The pull is capable of changing the orientation of the convergence related stresses, the principal axes will rotate, especially when the convergence is relatively weak.

6.1.3. Combination of gravitational spreading forces and convergence

The results in section 5.1.3. show that the Alboran Domain needs to be of a height of 2000m (Fig. 18) to be able to produce normal faulting at the crest. This value is only of limited interest because, as explained, the actual lithospheric structure is likely to have been different from that assumed in the calculations. More relevant is the tensional force of ~2.4 x 10^{12} Nm^{-1}, as calculated in the results.

The compression due to convergence is very effective in compensating the tension, due to a similar orientation. The gravitational potential energy contrast of ~5.1 x 10^{12} Nm^{-1}, calculated by (Platt et al., 2003), which is higher than the contrast used in my models, would be sufficient to withstand the compensating compression. A different effect of the similar orientation is the increase of tension in SW-NE orientation. This orientation favors the tension due to roll-back related pull, which is probably why the tension is so pronounced when the Alboran Domain is also under compressional stress from the convergence. The tension of the pull is augmented by that of the Domain.

6.1.4. Combination of gravitational spreading forces and roll-back related pull

When combining the Alboran Domain high with a roll-back related pull of similar magnitude (5.1.4.), it is clear that the principal axes are slightly rotated towards the internal boundary, but that the NW-SE tension is still present in the Alboran Domain. The magnitude of the SW-NE tension is increased compared to that of the original field (Fig. 12), which is due to a weak E-W contribution of the high itself, as describe before. Both these tensional orientations are evidenced in the field.

Early Miocene stretching lineations have been found in the Internal Betics (Fig. 32). Their shear sense support two stages of exhumation. An early synkinematic with sillimanite stage towards the ENE, and a late synkinematic with andalusite stage towards the north. The first can be related to the roll-back related pull or the westward motion of the Alboran Domain, while the second can be related to the gravitational spreading of the Alboran Domain.

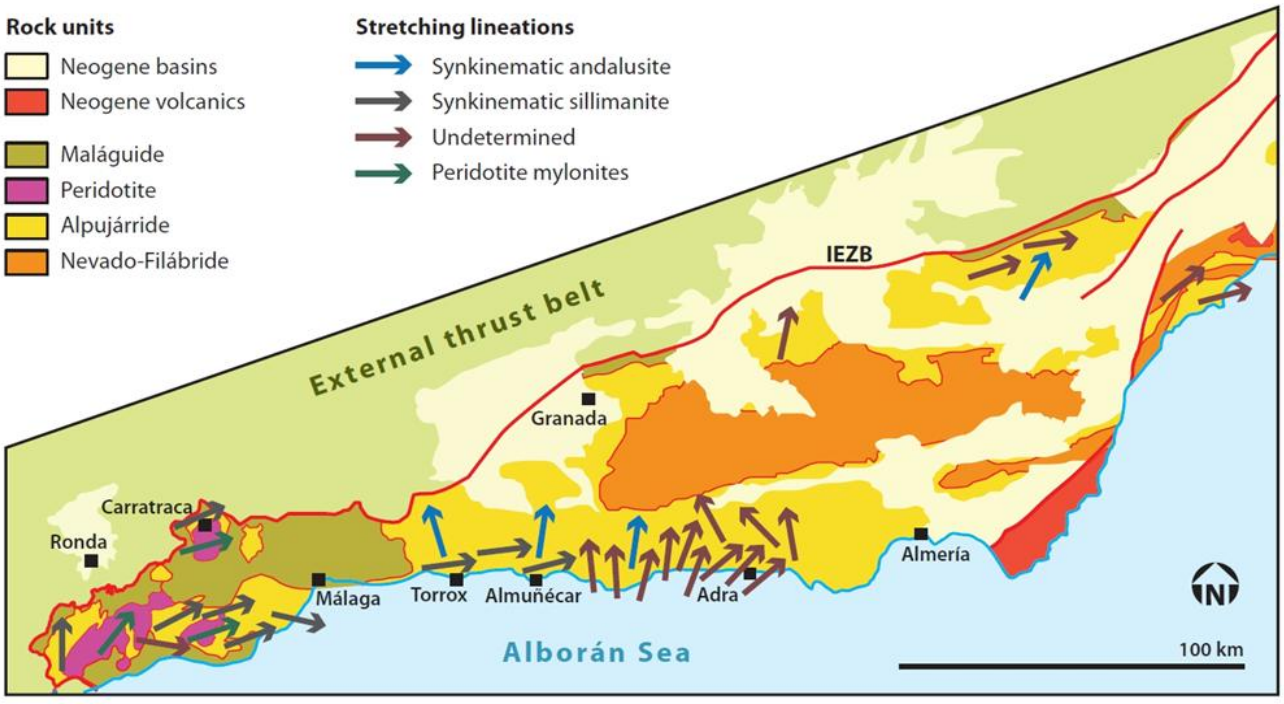

Figure 32: Kinematics of early Miocene extension in the Alpujaridde Complex (Platt et al., 2013). *Especially the synkinematic sillimanite (grey arrows) and synkinematic andalusite (blue arrows) are of interest, because they can indicate a first ENE extensional stage related to slab roll-back or westward motion of the Alboran Domain and a second stage of thrusting due to gravitational spreading.*

6.1.5. Combining all three involved tectonic forces

In general, looking at the combination of all three forces (5.1.5.), the convergence may seem to be the most dominant factor, but in my model the contribution of convergence may have been overestimated. I only look at relative relations between the forces, and maybe my extremes are not extreme enough. For example, the Alboran Domain of 2000m high and a associated force of ~2.4 * 10^{12} Nm^{-1} is in balance with the convergence of 2 * 10^{12} Nm^{-1}, but other values may give a more realistic gravitational potential energy contrast as calculated by Platt et al. (2003), although their calculation is based on a Alboran Domain of 19 Ma.

The purpose of the model analysis was to show the first-order relationships between the various forces. In addition to the previous, several things stand out in the model results.

One of those things is that when the Alboran Domain of 2000m high is in balance with the convergence of 2 * 10^{12} Nm^{-1}, a zone with a neutral state of stress develops which is sensitive to the roll-back related pull. The increased tension, due to the augmented effect of the pull and the Domain, could be a possible cause for a delay of the onset of the Messinian Salinity Crisis as suggested by Jolivet et al. (2006). The combination of all three forces with a moderate magnitude can be regarded as a first step in the evolution, preceding the onset of the MSC. Previous to this step the GPE contrast was probably even higher, so that the main thrusting could take place.

Due to the zone with a neutral state of stress, the effect of a termination of the roll-back related pull will also be more prominent in the stress field. The roll-back related pull ceased 2Myr before the onset of the MSC (Jolivet et al., 2006) and the Alboran Domain decreased in height as well (Comas et al., 1999), which is not necessarily relevant but could indicate a decrease in potential energy, causing the convergence to be the dominant factor and the whole area to be in compression. This stage of overall compression could be the cause of the closure of the two remaining connections with the Atlantic. Gutscher et al. (2002) suggest that the tectonic evolution of the Betic-Rif arc is ongoing and may take the form of an active east-dipping subduction zone in the Gulf of Cadiz. Therefore I think that a reactivation of the roll-back related pull is justified and this could be the cause of re-opening the connection with the Atlantic, but because of the decrease and maybe even disappearance of the Alboran Domain, this pull creates only tension near the internal boundary, near the Strait of Gibraltar. The rest of the field is still under compression, which can cause the Alboran Domain to be inverted. This can also be seen some parts of the Alhama de Murcia fault, which reactivated as contraction faults during the latest Miocene to early Pliocene in response to the continuing of the African-Eurasia convergence (Meijninger & Vissers, 2006).

A temporary cessation of roll-back has been suggested to have occurred, caused by the slab arriving at the 660k discontinuity in the mantle, as suggested by Faccenna et al. (2001), who show a similar result in an analogue experiment. Such a halt occurred as well in the opening of the Liguro-provencal basin and in a second phase the opening of the Tyrrhenian basin. Mantle material cannot flow poloidal anymore, it takes some time to change the regime to toroidal flow only, allowing the slab to retreat again. Toroidal flow can enhance the extension in the overriding plate according to Schellart & Moresi (2013).

6.1.6. Model limitations

This description of the geological evolution is highly speculative but does illustrate that a numerical model can contribute to the general understanding of the area. Boundary conditions on the magnitude, distribution and orientation of the forces need to be refined in future work. Also, insight into the relative timing of the appearance of these forces is needed. Once this information is available maybe a more regional case study can be tested using the model.

Other limitations of the model discussed in this report are the uniform thicknesses of the plate, these could be changed to more realistic values. No thermal parameters are included either, and the model is elastic, so we are not able to follow the deformation over time. These limitations are also applicable to the model of the Eastern Pyrenees, discussed in the next session.

6.2 Eastern Pyrenees

The superposition of a relatively small area with an increased gravitational potential energy forms a first-order approximation of the dynamic effects of a missing lithospheric root. The exact shape and magnitude are of second order interest; two possibilities are tested and shown in section 5.2.

The anti-clockwise rotation of the tension by ~20 degrees results in normal faulting with a similar orientation as the normal faults bounding the relatively young extensional basins in the area (see Fig. 3), for instance the Emporda and La Selva basins (late Miocene to recent age (Lewis et al., 2000)). This could confirm that the second phase of extension in the area described by Gunnell et al. (2008) is indeed related to an additional phase of uplift in the Eastern Pyrenees.

According to the model results, tensional stresses with a similar orientation appear NE of the imposed high as well, but normal faults with a NW-SE strike are not visible at that location in the field (see Fig. 3). The shape of the high is thus maybe not entirely realistic, it could be that the lithospheric root is delaminated more to the south explaining in the absence of normal faults to the NE in reality. Incorporating an asymmetric shape or even a change of position towards the south could be a more realistic setup of the model. Root erosion has so far been comparatively more intense in the Eastern than the Central Pyrenees because the east has been exposed to a greater number of potential heat sources (Gunnell et al., 2008). The observed migration of volcanism to the SW can be supportive evidence for the migration of delamination of the mantle lithosphere (Lewis et al., 2000).

The orientation of convergence is the most important factor controlling the direction of tension in the high, as well as the deflection surrounding the high. The higher the amount of uplift, the larger the deflections will be. The model of the Eastern Pyrenees is still a quite limited one, other forces could be introduced to get a more complete model. For instance the subduction of the northern Apennines could have played a role, causing an additional tensional force to the NE with respect to the Pyrenees, although this force is probably limited during the Late Miocene, see figure 33 (Carminati et al., 1998). This figure shows that there are only very small stresses present in the Eastern Pyrenees.

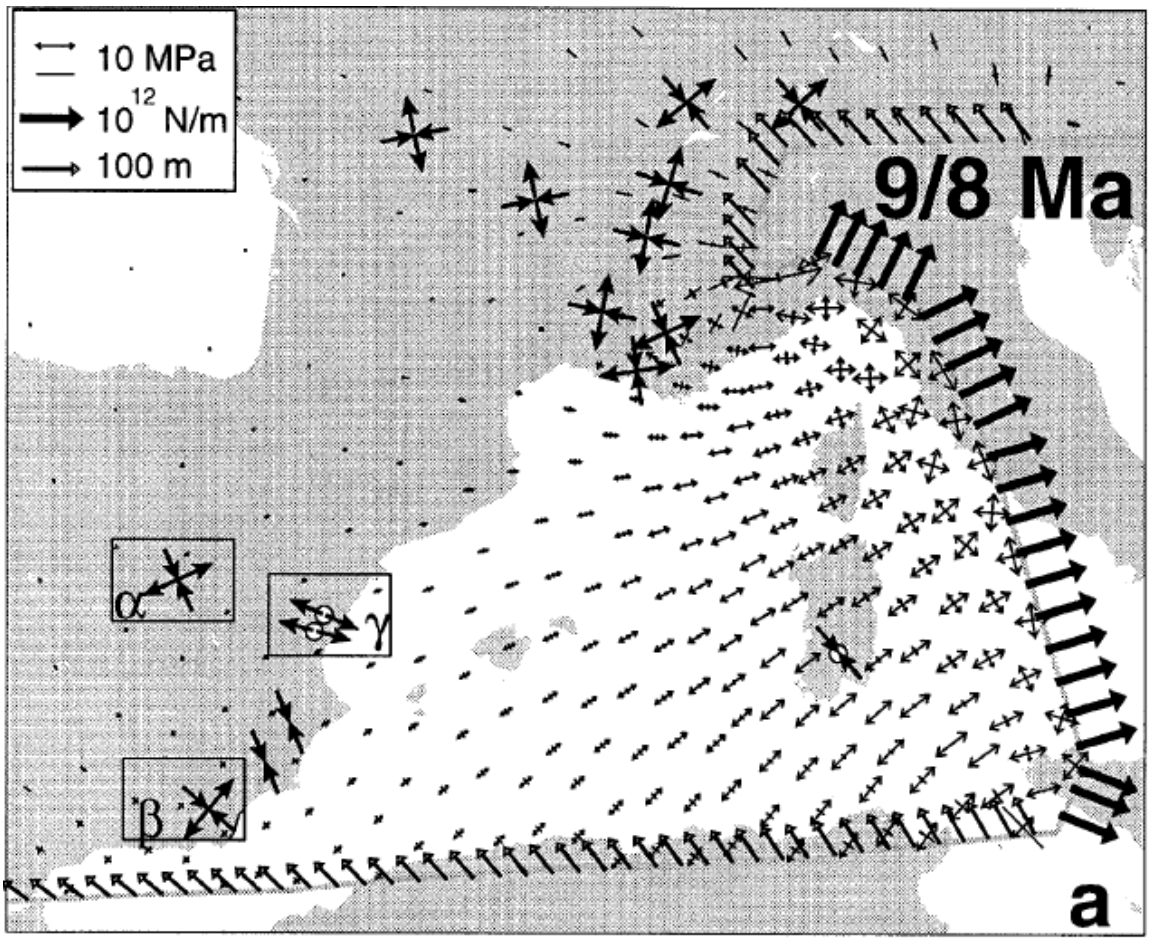

Figure 33: Intra-plate stress field calculated with a model referring to the Tortonian opening stage of the Tyrrhenian basin (Carminati et al., 1998). The subduction of the northern Apennines results in a additional little E-W tensional stress in the Eastern Pyrenees.

6.3 Future research

Additional research in the Betic region which uses a similar approach should focus on more realistic boundary conditions to be able to compare the results with geological data on smaller scale. Improved understanding of the kinematics will require collection of palaeomagnetic data and thrust slip vectors from the external northern Rif, for which data are largely lacking (Platt et al., 2013). Other components should be added to get a complete picture of the area, like an Atlantic ridge-push force or the incorporation of differences in crustal and mantle thickness. A model which is influenced by lithospheric rebound due to evaporites deposition would be a nice expansion of the Messinian model (Govers et al., 2009). Furthermore, a model with present boundaries should be designed to test if the field resembles the present-day stress field, when all topographic highs as potential energy sources are taken into account.

7. Conclusion

The Betic region has been influenced during the Miocene by a NNW-SSE convergence, a westward directing pull related to roll-back and an extension due to the increased potential energy of the Alboran Domain. With a finite element elastic thin shell model I focused on the relative importance of these forces. Additionally I looked at a solution for the anomalously high elevation of the Eastern Pyrenees in a similar fashion.

Based on the model results the following conclusions can be made:

1) Timing of the existence of each force is very important in controlling the geometry of the stress-pattern in the area.

2) Convergence needs to be relative weak in order to see an effect due to one of the other two forces. The convergence is the most dominant factor, followed by the increased potential energy of the Alboran Domain. Tension caused by the roll-back related pull does not reach that far into the Domain, the pull has the weakest contribution.

3) The Alboran Domain and convergence should be in balance to create a zone with a neutral state of stress which is extra vulnerable to the roll-back related pull. If one of the two will change, the pull will not have that much of an effect. A maximum WSW-ENE tension will occur when both a neutral state of stress and a pull is present. Therefore, it is not possible to distinguish between slab roll-back and an increased GPE as the main driving force in the area, a combination is needed.

4) The temporary cessation of the roll-back related pull in combination with a decreasing energy potential of the Alboran Domain results in a compressive field due to the convergence. This phase of compression could be responsible for the closure of the Betic and Rifian corridors to the Atlantic, inducing the MSC.

5) The stress pattern induced by a small area with increased potential energy located in the Eastern Pyrenees in combination with the general convergence field confirms that the existence of the Miocene basins and volcanism in the field can be related to an additional extensional phase during the Late Miocene.

8. Acknowledgement

I would like to thank Paul Meijer for his eternal patience answering my questions and helping me in any other way to solve my problems. I also owe thanks to Rob Govers, who created GTecton, without this program I would not be able to create my model. The same goes for the programs Triangle and GMT.

9. References

Beatty, M. (1977), Vector analysis of finite rigid rotations. Journal of Applied Mechanics 44, pp.501.

Bezada, M., E. Humphreys, D. Toomey et al. (2013), Evidence for slab rollback in westernmost Mediterranean from improved upper mantle imaging. Earth and Planetary Science Letters 368, pp.51-60.

Bird, P. (2003), An updated digital model of plate boundaries. Geochemistry Geophysics Geosystems 4(3), pp.1027.

Boyden, J.A., R.D. Müller, M. Gurnis et al. (2011), Next-generation plate-tectonic reconstructions using GPlates. Geoinformatics: Cyberinfrastructure for the Solid Earth Sciences, pp.95-114.

Calais, E., C. DeMets & J. Nocquet. (2003), Evidence for a post-3.16-Ma change in Nubia–Eurasia–North America plate motions? Earth and Planetary Science Letters 216(1), pp.81-92.

Carminati, E., M. Wortel, P.T. Meijer et al. (1998), The two-stage opening of the western–central Mediterranean basins: a forward modeling test to a new evolutionary model. Earth and Planetary Science Letters 160(3), pp.667-679.

Comas, M., J. Platt, J. Soto et al. (1999). 44. the origin and tectonic history of the alboran basin: Insights from leg 161 results. Paper presented at the Proceedings of the Ocean Drilling Program Scientific Results, , 161 pp.555-580.

Duggen, S., K. Hoernle, P. van den Bogaard et al. (2004), Magmatic evolution of the Alboran region: The role of subduction in forming the western Mediterranean and causing the Messinian Salinity Crisis. Earth and Planetary Science Letters 218(1), pp.91-108.

Duggen, S., K. Hoernle, d.B. van et al. (2003), Deep roots of the Messinian salinity crisis. Nature 422(6932), pp.602.

England, P. & G. Houseman. (1989), Extension during continental convergence, with application to the Tibetan Plateau. Journal of Geophysical Research: Solid Earth (1978–2012) 94(B12), pp.17561-17579.

Faccenna, C., F. Funiciello, D. Giardini et al. (2001), Episodic back-arc extension during restricted mantle convection in the Central Mediterranean. Earth and Planetary Science Letters 187(1–2), pp.105-116.

Govers, R., P. Meijer & W. Krijgsman. (2009), Regional isostatic response to Messinian Salinity Crisis events. Tectonophysics 463(1), pp.109-129.

Gunnell, Y., H. Zeyen & M. Calvet. (2008), Geophysical evidence of a missing lithospheric root beneath the Eastern Pyrenees: Consequences for post-orogenic uplift and associated geomorphic signatures. Earth and Planetary Science Letters 276(3–4), pp.302-313.

Gutscher, M., J. Malod, J. Rehault et al. (2002), Evidence for active subduction beneath Gibraltar. Geology 30(12), pp.1071-1074.

Hsü, K.J., L. Montadert, D. Bernoulli et al. (1977), History of the Mediterranean salinity crisis. Nature 267(5610), pp.399-403.

Jolivet, L., R. Augier, C. Robin et al. (2006), Lithospheric-scale geodynamic context of the Messinian salinity crisis. Sedimentary Geology 188–189(0), pp.9-33.

Jolivet, L. & C. Faccenna. (2000), Mediterranean extension and the Africa-Eurasia collision. Tectonics 19(6), pp.1095-1106.

Krijgsman, W., F. Hilgen, I. Raffi et al. (1999), Chronology, causes and progression of the Messinian salinity crisis. Nature 400, pp.652-655.

Krijgsman, W. & M. Garces. (2004), Palaeomagnetic constraints on the geodynamic evolution of the Gibraltar Arc. Terra Nova 16(5), pp.281-287.

Lewis, C.J., J. Vergés & M. Marzo. (2000), High mountains in a zone of extended crust: Insights into the Neogene-Quaternary topographic development of northeastern Iberia. Tectonics 19(1), pp.86-102.

Lonergan, L. & N. White. (1997), Origin of the Betic-Rif mountain belt. Tectonics 16(3), pp.504-522.

Martínez-Martínez, J. & J. Azañón. (1997), Mode of extensional tectonics in the southeastern Betics (SE Spain): Implications for the tectonic evolution of the peri-Alborán orogenic system. Tectonics 16(2), pp.205-225.

Mauffret, A., B. Durand de Grossouvre, A. Tadeu Dos Reis et al. (2001), Structural geometry in the eastern Pyrenees and western Gulf of Lion (Western Mediterranean). Journal of Structural Geology 23(11), pp.1701-1726.

Meijer, P.T. (1995), Dynamics of active continental margins: the Andes and the Aegean region. Geologica Ultraiectina 130, pp.1-218.

Meijninger, B. & R. Vissers. (2006), Miocene extensional basin development in the Betic Cordillera, SE Spain revealed through analysis of the Alhama de Murcia and Crevillente Faults. Basin Research 18(4), pp.547-571.

Molnar, P. & H. Lyon-Caen. (1988), Some simple physical aspects of the support, structure, and evolution of mountain belts. Geological Society of America Special Papers 218, pp.179-208.

Platt, J. (2007), From orogenic hinterlands to Mediterranean-style back-arc basins: a comparative analysis. Journal of the Geological Society 164(2), pp.297-311.

Platt, J., S. Allerton, A. Kirker et al. (2003), The ultimate arc: Differential displacement, oroclinal bending, and vertical axis rotation in the External Betic-Rif arc. Tectonics 22(3), pp.1017.

Platt, J., J. Soto, M. Whitehouse et al. (1998), Thermal evolution, rate of exhumation, and tectonic significance of metamorphic rocks from the floor of the Alboran extensional basin, western Mediterranean. Tectonics 17(5), pp.671-689.

Platt, J., W. Behr, K. Johanesen, J.Williams. (2013), The Betic-Rif Arc and Its Orogenic Hinterland: A Review. Annu. Rev. Earth Planet. Sci.(41), pp.313-357.

Rosenbaum, G., G.S. Lister & C. Duboz. (2002), Relative motions of Africa, Iberia and Europe during Alpine orogeny. Tectonophysics 359(1), pp.117-129.

Schellart, W. & L. Moresi. (2013), A new driving mechanism for backarc extension and backarc shortening through slab sinking induced toroidal and poloidal mantle flow: Results from dynamic subduction models with an overriding plate. Journal of Geophysical Research: Solid Earth

Sissingh, W., W. Autin, H. Kombrink et al. (2008), Punctuated Neogene tectonics and stratigraphy of the African-Iberian plate-boundary zone: concurrent development of Betic-Rif basins (southern Spain, northern Morocco). Netherlands Journal of Geosciences-Geologie en Mijnbouw 87(4), pp.241.

Spakman, W. & R. Wortel. (2004). A tomographic view on western mediterranean geodynamics. The TRANSMED atlas. The Mediterranean region from crust to mantlepp. 31-52Springer.

Vergés, J., M. Fernàndez & A. Martínez. (2002), The Pyrenean orogen: pre-, syn-, and post-collisional evolution. Journal of the Virtual Explorer 8, pp.57-76.

Vissers, R., J. Platt & D. Van der Wal. (1995), Late orogenic extension of the Betic Cordillera and the Alboran Domain: A lithospheric view. Tectonics 14(4), pp.786-803.

Vissers, R.L.M. (2012),
Extension in a convergent tectonic setting:
a lithospheric view on the Alboran system of SW Europe.

Vissers, R.L.M. & P.T. Meijer. (2012), Iberian plate kinematics and Alpine collision in the Pyrenees. Earth-Science Reviews 114(1–2), pp.61-83.

Watts, A.B., J.P. Platt & P. Buhl. (1993),
Tectonic evolution of the Alboran Sea
basin. Basin Research(5), pp.153-177.

Wessel, P. & W.H. Smith. (1991), Free software helps map and display data. Eos, Transactions American Geophysical Union 72(41), pp.441-446.

Zeyen, H. & M. Fernàndez. (1994), Integrated lithospheric modeling combining thermal, gravity, and local isostasy analysis: Application to the NE Spanish Geotransect. Journal of Geophysical Research: Solid Earth (1978–2012) 99(B9), pp.18089-18102.

Zienkiewicz, O. C. & Taylor, R. L. (1977). The finite element method. McGraw-hill London.

10. Appendices

Appendix A: Calculation sum of rotations

Here I will explain the method I used to define the rotation pole used in my model.

The two original rotation poles are:

$R^{0,19.589}$ = lat. -21.54; long. 166.42, angle 1.9880 (R. L. M. Vissers & Meijer, 2012).

and

$R^{3,0}$ = lat. 19.3; long. -19.0; rate 0.103°/Ma (Calais et al., 2003).

The notation $R^{3,0}$ is used to define the rotation from 3 Ma to present. So $R^{0,19.589}$ defines a reconstruction pole from present to 19.589 Myr ago. The objective is to find a pole for the Middle to Late Miocene, therefore the Calais pole which describes the last 3 Myr is subtracted from the Vissers & Meijer (2012) pole, like this:

$$R^{19.589,\,3} = R^{19.589,0} + R^{0,3}$$
$$= (-1 * R^{0,19.589}) + (-1 * R^{3,0})$$
$$= (-21.54; 166.42; -1.9880) + (19.3; -19.0; -0.309)$$

This is possible due to the fact that the poles are finite rotations. Euler's Displacement Theorem states that any displacement of a rigid body (which we assume tectonic plates are), is a rotation about some axis through that point (Beatty, 1977). A negative angle of rotation is used to calculate the pole back in time. The rate of Calais et al. (2003) first needs to be multiplied by 3Myr to convert to an angle.

We can now add the poles by matrix multiplication, described in the following method:

Rotation 1: Pole at latitude L1, longitude W1, Rotation angle A1.

$\cos A1/2 = a1$
$\sin A1/2 \cos L1 \cos W1 = b1$
$\sin A1/2 \cos L1 \sin W1 = c1$
$\sin A1/2 \sin L1 = d1$

The notation a1 to d1 is used in the following calculations.

The same method applies to rotation 2. Now apply matrix multiplication. The result of the two rotations is:

(a1a2 - b1b2 - c1c2- d1d2) = a
(a1b2 + a2b1) + (c2d1 - c1d2) = b
(a1c2 + a2c1) + (d2b1 - d1b2) = c
(a1d2 + a2d1) + (b2c1 - b1c2) = d

To find the new pole use:

Rotation angle A = 2 arccos a
Latitude L = arcsin (d/sin A/2)
Longitude W = arctan (c/b)

To obtain an accurate results, 8 digits are required in the calculation.

Appendix B: Choice pole of rotation

The next three figures display an enlarged stress field, to show the different response of the field to the choice of the several rotation poles, which can be seen in figure 8.

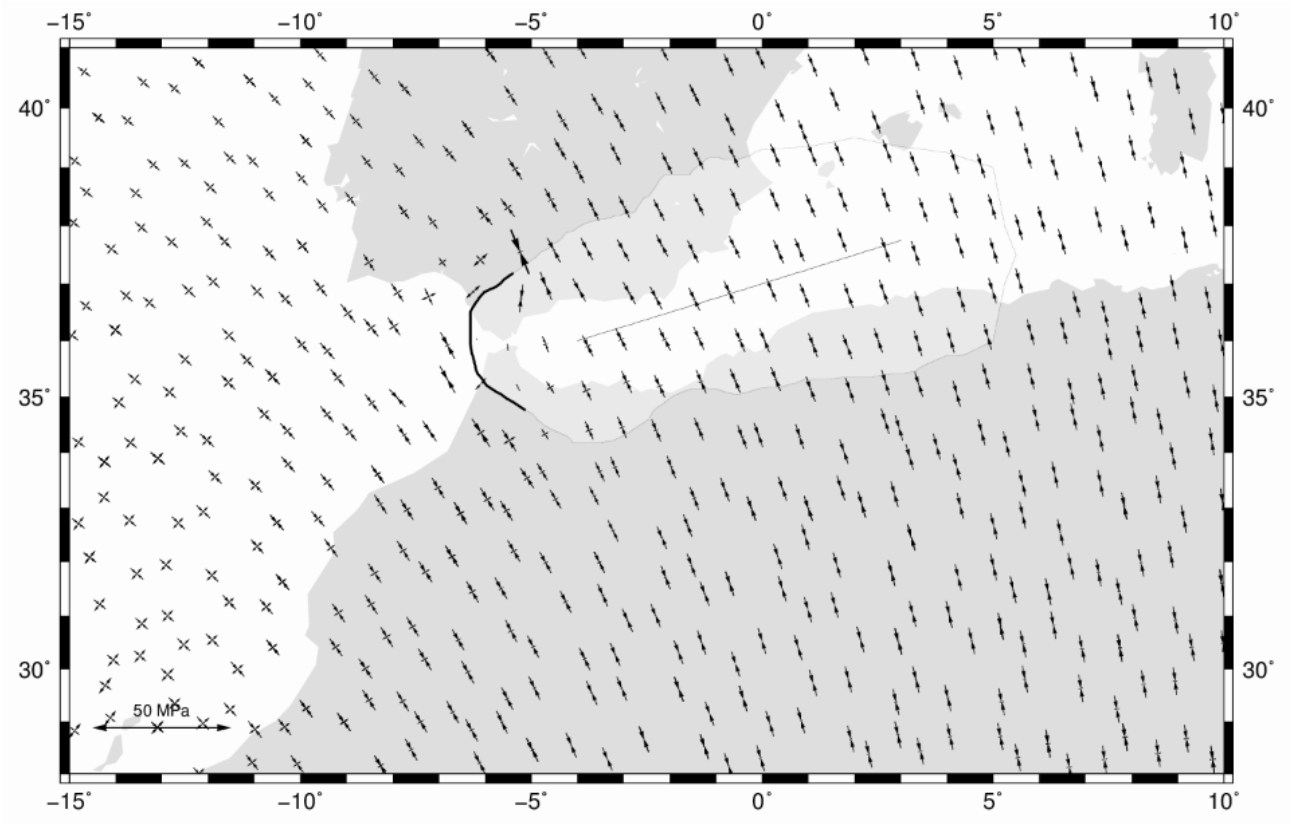

Figure B1: Stress field induced by the combination of poles (Fig.8 black arrows). This response to the convergence is used in all other models.

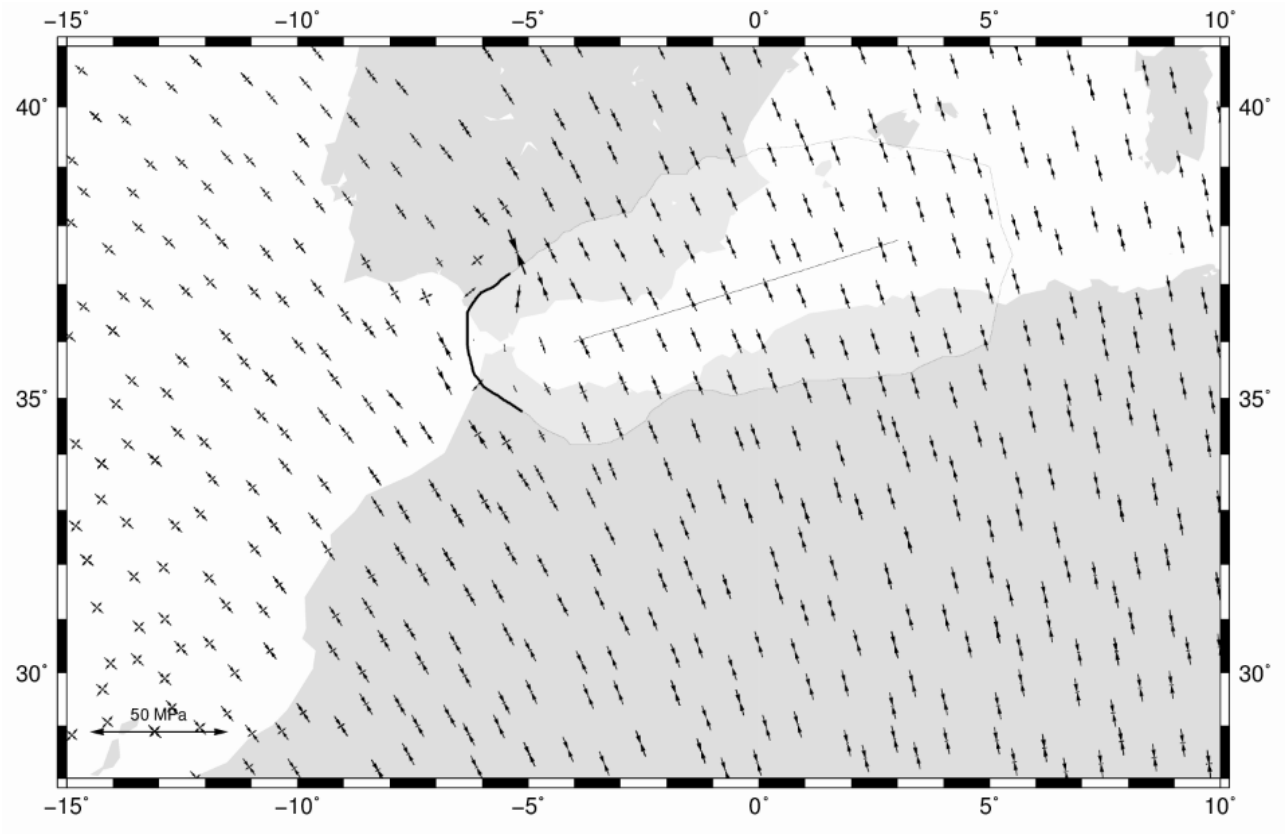

Figure B2: Stress field induced by the pole of Vissers & Meijer (2012) (Fig.8 blue arrows). This response resembles that of B1.

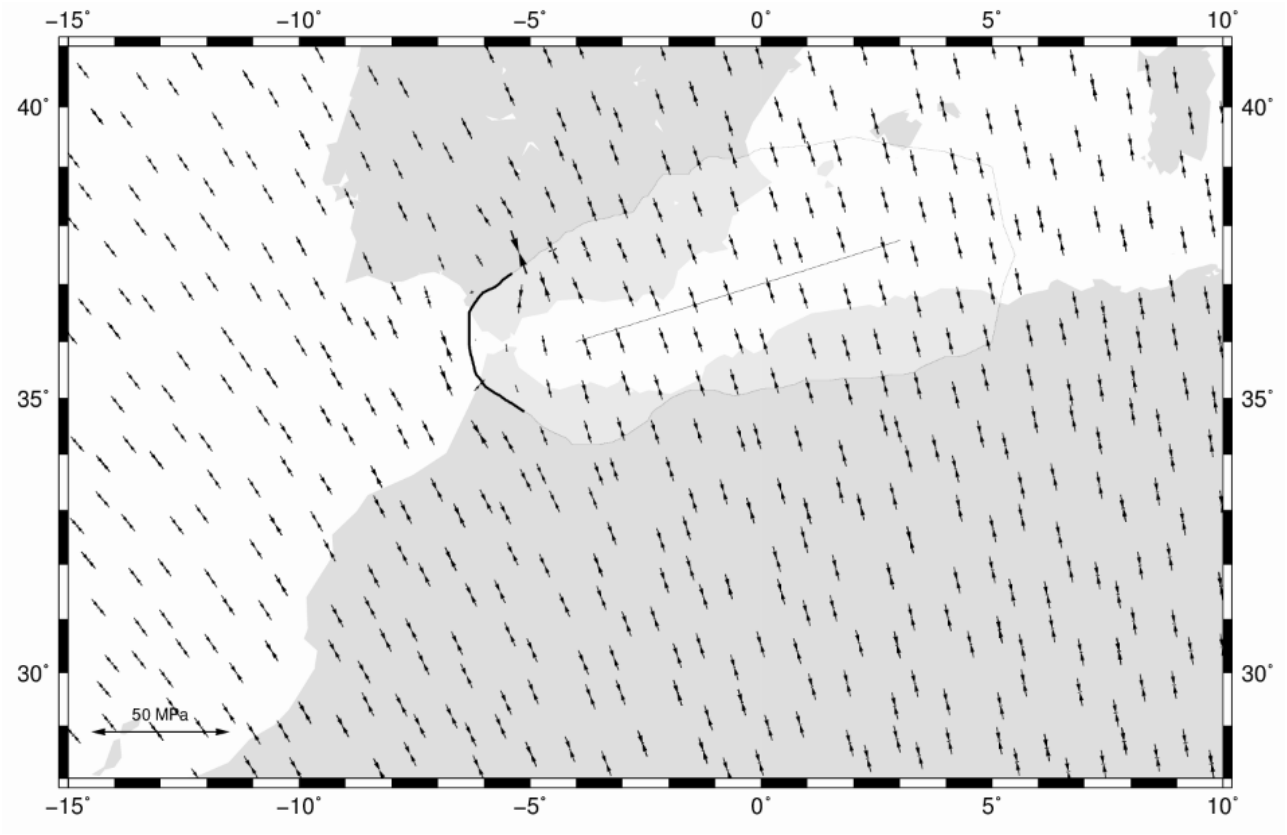

Figure B3: Stress field induced by the pole of Calais et al. (2003) (Fig.8 blue arrows). The main difference with C1 & C2 is: no tension in NE-SW orientation. Nevertheless inside the area of interest, surrounded by the contour of the Alboran Domain, the differences are very small: slight change in orientation overall (less than 5 degrees), and lack of very small NE-SW tension in the western part of this area.

Appendix C: Extending uncoupled internal boundary

Here the differences in stress field are shown in response to a north-eastward extension of the uncoupled internal boundary combined with additional roll-back related pull acting on this boundary.

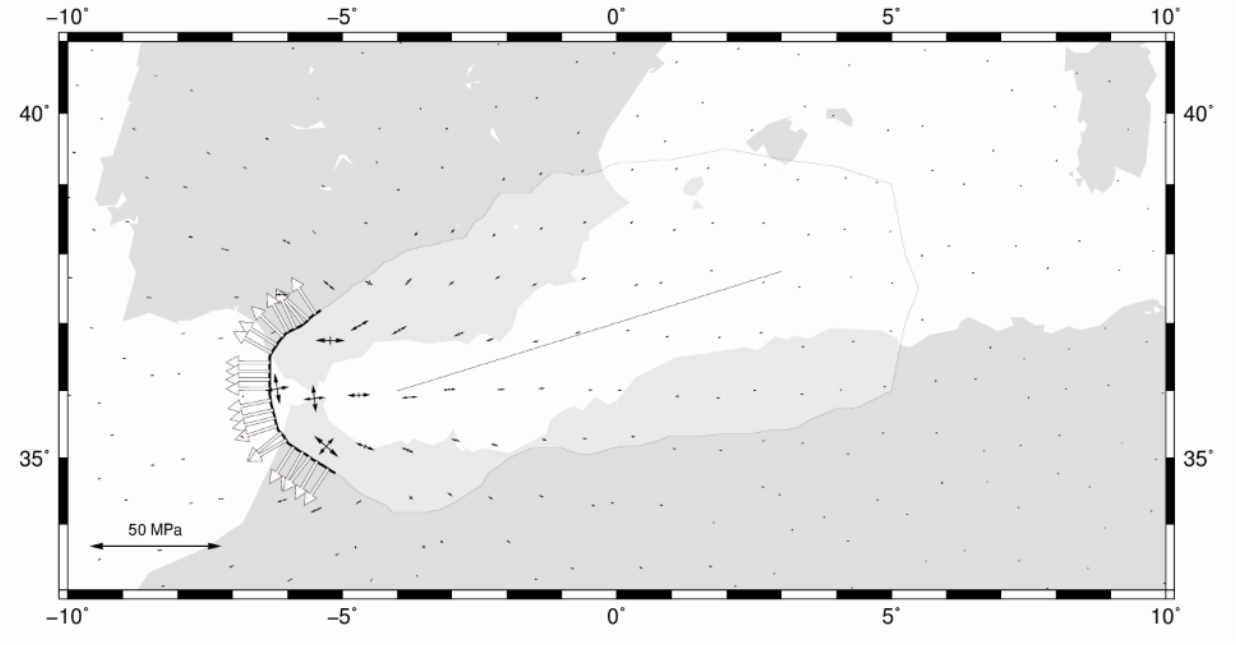

Figure C1: Original model R8, only force acting on the stress field is the westward acting pull.

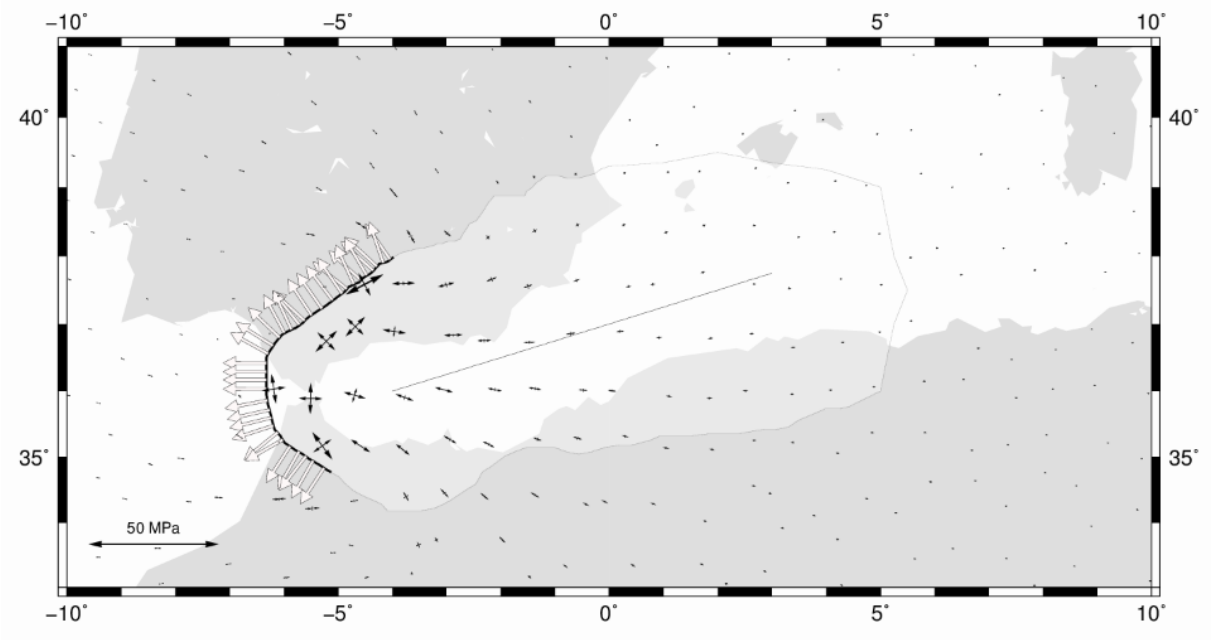

Figure C2: Similar to C1, except now the uncoupled boundary as well as the pull continues to the northeast. Increased pull increases tensional forces within AD. There is also a small rotation of the field to the north.

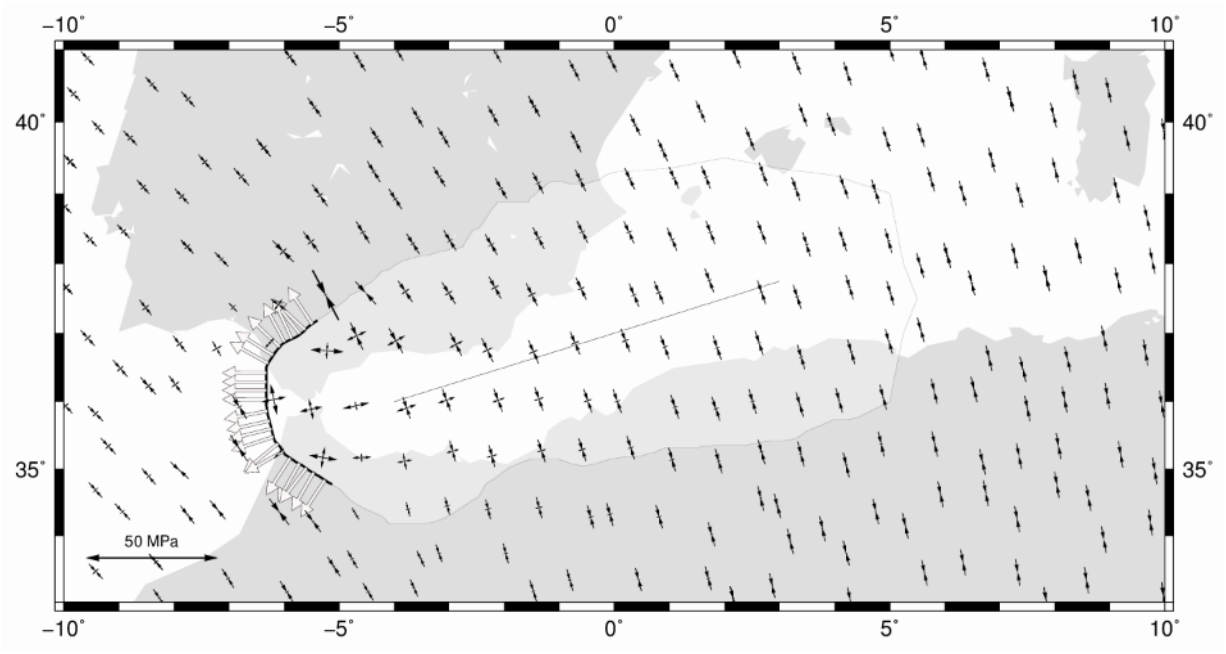

Figure C3: Original model R6, two forces acting on the stress field: the westward acting pull and Africa-Eurasia convergence with a ratio of 1 to 1.

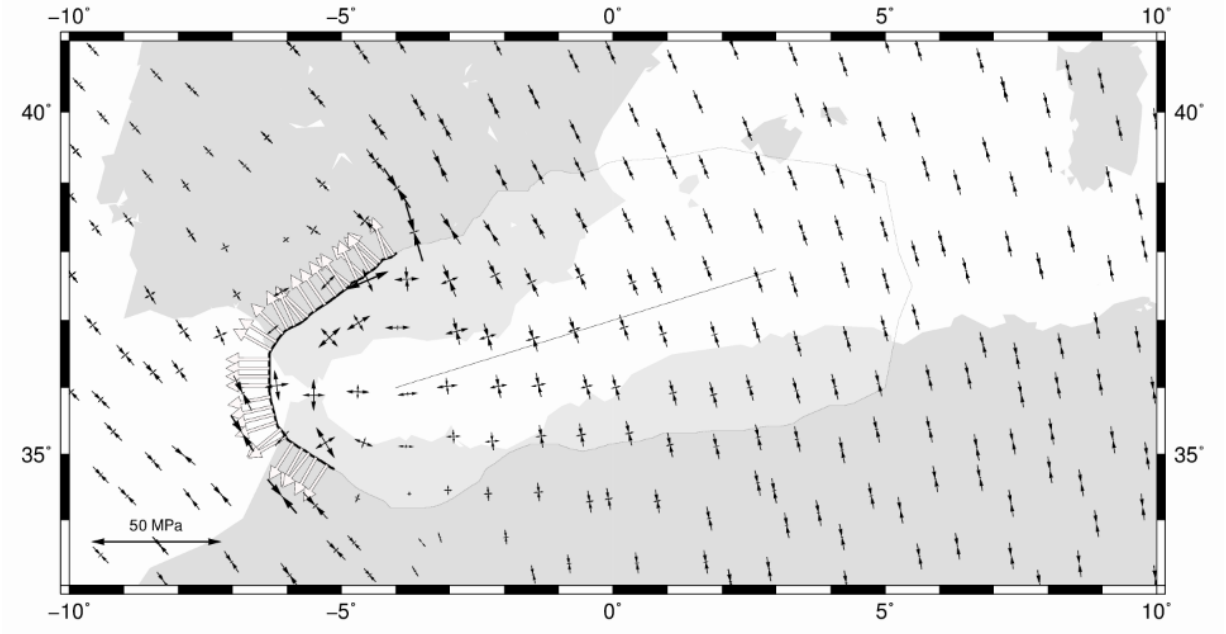

Figure C4: Similar to C3, except now the uncoupled boundary as well as the pull continues to the northeast. Main differences are the enlarging of the 'shadow zone' and shifting of the edge effects surrounding the northeastern tip of the uncoupled boundary.

Appendix D: Tables of results

The following tables describe all possible combinations of the tectonics forces applied in each model experiment. Abbreviations: AD = Alboran Domain, this gives the height of the crest of the Alboran Domain; Conv = Convergence applied at the southern boundary; Pull = Roll-back related pull, this describes the magnitude of pull at the western internal boundary of the Alboran Domain. Both convergence and roll-back related pull are in units of 10^{12} Nm^{-1}. Each experiment has a different number, if this number has a bold font, the run is shown in this work.

AD 0m	Conv x2	Conv x1	Conv x0.5	Conv x0
Pull x2	**R1**	R2	**R3**	**R4**
Pull x1	R5	R6	R7	R8
Pull x0.5	R9	**R10**	R11	R12
Pull x0	**R13**	R14	R15	R16

AD 500m	Conv x2	Conv x1	Conv x0.5	Conv x0
Pull x2	R17	R18	R19	**R20**
Pull x1	R21	R22	R23	R24
Pull x0.5	R25	R26	R27	R28
Pull x0	R29	**R30**	R31	R32

AD 1000m	Conv x2	Conv x1	Conv x0.5	Conv x0
Pull x2	R33	R34	R35	R36
Pull x1	R37	**R38**	R39	R40
Pull x0.5	R41	R42	R43	R44
Pull x0	R45	R46	R47	R48

AD 2000m	Conv x2	Conv x1	Conv x0.5	Conv x0
Pull x2	**R49**	R50	R51	**R52**
Pull x1	R53	R54	R55	R56
Pull x0.5	R57	R58	R59	**R60**
Pull x0	**R61**	**R62**	**R63**	**R64**

Pyrenees	1000m	2000m
No convergence	**P1**	**P3**
Convergence	**P2**	**P4**